Investigation and Optimisation of a Multi Cyclone Separation System

A Comprehensive Study on the Effects of Design and Operation Parameters on Separation Efficiency For a High Efficiency Stairmand Cyclone

Christian Troue Lynderup Jensen & Jonas Carbuhn Bendtsen

Thermal Energy and Process Engineering, TEPE4-1004

Masters Project

AALBORG UNIVERSITY
STUDENT REPORT

This report is made in LATeX. Mathematical calculations are made using Engineering Equation Solver (EES), and Ansys Fluent is used for all CFD simulations. The 3D drawing are made in FreeCAD. Visio and Draw.io is used for designing various figures, and Python has been utilised for plots and graphs throughout the project.

Title:

Investigation and Optimisation of a Multi Cyclone Separation System

Theme:

Cyclone Particle Filtration

Project Period:

Spring Semester 2024

Project Group:

TEPE4-1004

Participants:

Christian Troue Lynderup Jensen

Jonas Carbuhn Bendtsen

Supervisors:

Kim Sørensen

Thomas Condra

Copies: 1

Page Numbers: 73

Date of Completion:

28. maj 2024

Abstract:

Filtration systems help mitigate health hazards by removing harmful particles from the air. This report investigates the performance of a High Efficiency Stairmand cyclone separator, how varying diameters, outlet designs and inlet velocities, affect backflow, pressure loss, and separation efficiency.

It was found that a bend on the outlet did not prevent backflow or significantly change separation efficiency, but merely increased the pressure loss. An decrease in vortex finder diameter showed to limit the backflow and increase the overall efficiency, but did not significantly change the fishhook and came at the cost of increased pressure loss. Additionally, modifying the cyclone diameter reveals that larger cyclones with lower inlet velocities in some cases can increase separation efficiency due to the fishhook effects, but reduced separation efficiency for larger particles. Conversely, smaller cyclones shows higher separation efficiency for larger particles but lower efficiency for fine particles. It was hypothesised that a series of cyclones with different design parameters can optimize overall separation efficiency and pressure loss by utilizing overlapping of the efficiency. This led to a design of a system consisting of one large and two small cyclones, with a minimum separation efficiency of 86.5% across particle diameters of 1-20μm.
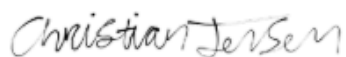
Contents

Preface

This project is written by 4. semester, Master students of group TEPE4-1004, studying Thermal Energy and Process Engineering. It is written in the period of 1. February to 31. may, 2024, under supervision of Kim Sørensen and Thomas Condra, to whom we extent our gratitude for their insight, feedback and guidance in this, as well as several other, projects throughout our education. Furthermore, we would like to thank Chungen Yin for his help and advice regarding various CFD simulations used in the project.

Aalborg University, May 28, 2024

Christian Troue Lynderup Jensen

<ctlj19@student.aau.dk>

Jonas Carbuhn Bendtsen

<jbendt19@student.aau.dk>

Resume

Filtreringssystemer anvendes ofte i produktionsindustrien til partikelfiltrering, især inden for træ- og metalindustrierne. Disse systemer er vigtige for at reducere sundhedsfarer ved at fjerne skadelige partikler fra luften. Der er adskillige metoder til at separere partikler fra luft, hver med deres egne fordele og begrænsninger. Cyklonseparatorer anvendes ofte til filtrering af større partikler på grund af deres enkle design, minimale vedligeholdelse og høje effektivitet. Nogle ventilationsfirmaer, som JKF-Industries i Hadsund, Danmark, bruger en cyklonseparator i serie med et luftposefilter for at fjerne størstedelen af de store partikler fra luften, hvilket reducerer behovet for vedligeholdelse af posefilteret. Det kan dog være fordelagtigt at undersøge muligheden for kun at bruge en teknologi og erstatte et posefilter med en eller flere cykloner.

I dette projekt blev en High Efficiency Stairmand cyklon modelleret og simuleret med CFD. Forskellige indløbshastigheder blev simuleret for at undersøge, hvordan dette påvirker tilbagestrømning, tryktab samt effektiviteten af cyklonen.

Effektivitets kurven for cyklonen viste at udskilningsgraden ved de lave partikel størrelser begyndte at stige igen. Dette er et kendt fænomen i cykloner kaldt "Fishhook" effekten. Det er stadig uvist hvorfor denne effekt forekommer, men flere teorier går på at det skyldes partiklernes påvirkning på hinanden. I dette projekt blev modellen simuleret uden partiklernes påvirkning på hinanden eller strømningen, og fishhook effekten forekom stadig. Det blev derfor undersøgt hvordan strømningen kunne have indflydelse på denne effekt.

Det blev blandt andet undersøgt om udløbsomstændighederne havde indflydelse på tryktabet, tilbageløbsstrømningen og udskilningseffektiviteten, med fokus på fishhook effekten. Det blev vist at en bøjning på udløbet ikke havde betydningsfuld indflydelse på tilbageløbsstrømningen eller udskilningseffektiviteten, men blot øgede tryktabet. En reduktion i udløbsrørets diameter viste at begrænsning i tilbageløbsstrømning og øge den samlede effektivitet. Det ændrede dog ikke fishhook effekten betydningsfuldt og øgede tryktabet. Derudover blev cyklonens diameter skaleret op og ned med varierende indløbshastigheder. Det blev konstateret, at dette kunne påvirke hvor Fishhook effekten forekommer, samt at fishhook effekten til en vis grad var skalerbar.

På baggrund af disse resultater blev det antaget, at en serie af cykloner med forskellige skaleringer og indløbshastigheder kan forbedre systemets samlede udskilningsgrad samt tryktab. Dette blev opnået ved at anvende Stokes skalering sammen med fishhook-effekten for at sikre overlapningen mellem de forskellige cykloners effektivitetskurver. Dette førte til et system bestående af en enkelt cyklon som førte over i to mindre. Dette gav et en minimums udskilningsgrad på 86.5% over en diameter spænd på 1-20μm. Derfor blev det konkluderet at, specielt for systemer med konstant volumetrisk strømning ville det være fordelagtigt at optimere et system der udnytter denne fishhook effekt.

Nomenclature

Abbreviation	Description
CFD	Computational Fluid Dynamics
CFL	Courant Friedrichs Lewy number
DPM	Discrete Phase Model
PM	Particle Matter
PRESTO	PREsure STaggering Option
RANS	Reynolds Average Navier Stokes
RNG	Renormalised Group
RSM	Reynolds Stress Model
SIMPLE	Semi-Implicit Method for Pressure-Linked Equations

Symbol	Description	SI unit
A_r	Surface Area of cyclone wall	[m^2]
D	Cyclone Diameter	[m]
D_p	Particle Diameter	[m]
D_x	Vortex Finder Diameter	[m]
F	Force	[N]
GCI_{fine}	Estimated solution error	[−]
H	Height	[m]
N_f	Number of cells in fine mesh	[−]
N_m	Number of cells in medium mesh	[−]
Q	Volumetric flow	[m^3/s]
R	Cyclone radius	[m]
Re	Reynolds number	[−]
Re_p	Particle Reynolds number	[−]
S	Length of vortex finder in cyclone	[m]
Stk	Stokes number	[−]
U	Free stream velocity	[m/s]
V	Volume	[m^3]
Y_d	Mass fraction	[−]

Nomenclature

Symbol	Beskrivelse	SI enhed
a	Height of cyclone inlet	[m]
b	Width of cyclone inlet	[m]
e_{mf}^a	Approximate Relative Error	$[-]$
f	Total Friction Factor	$[-]$
$f_{particles}$	Particle Friction Factor	$[-]$
f_{wall}	Wall Friction Factor	$[-]$
g	Gravitational Acceleration	$[m/s^2]$
k	Euler number	$[-]$
k	Turbulent kinetic energy	$[m^2/s^2]$
k_p	Turbulent kinetic energy near the wall node	$[-]$
m	Slope factor	$[-]$
$\dot{m}$	Mass flow	[kg/s]
p	Apparent Order	$[-]$
p	Pressure	[Pa]
r	Radius	[m]
t	Time	[s]
t_{res}	Particle residence time	[s]
u'	Fluctuating velocity	[m/s]
v	Velocity	[m/s]
v_{avg}	Average velocity	[m/s]
v_{ch}	Characteristic velocity	[m/s]
x_{50}	Cut Size	[m]
x_{fact}	Correction Factor	$[-]$
x_i	Particle diameter	[m]

Nomenclature

Symbol	Beskrivelse	SI enhed
α_p	Particle volume fraction	$[-]$
$\bar{\tau}$	Stress tensor	$[\text{Pa}]$
ϵ	Turbulence dispersion Rate	$[\text{m}^2/\text{s}^3]$
η	Efficiency	$[-]$
μ	Dynamic viscosity	$[\text{kg}/\text{m} \cdot \text{s}]$
ω	Characteristic swirl number	$[-]$
ϕ	Cell Value	$[-]$
ϕ_{mf}^{ext}	Extrapolated exact solution	$[-]$
ρ_f	Fluid density	$[\text{kg}/\text{m}^3]$
ρ_p	Particle density	$[\text{kg}/\text{m}^3]$
τ_f	Characteristic time of the flow	$[\text{s}]$
τ_v	Particle momentum response Time	$[\text{s}]$

1 Introduction

Ventilation is widely used in various production industries, a considerable part of which, is used for particle filtration. Manufacturers in the wood and metal industry use dust extraction systems to remove particles, in order to prevent health hazards due to inhalation. The particles in the air are then filtered to a certain level before either released into the atmosphere or used for heat recovery or directly reentered into the production facility. A considerable part of the particle emissions to the atmosphere comes from the wood processing industry.

According to numbers presented by Energi [8], approximately 13% of the coarse particles in the air comes from industrial processes, with 1400 companies in Denmark emitting wood dust and particles.

There are several methods used to separate particles from air, each of which have their own advantages and limitations. Cyclone separators is often used for air filtration for larger particles, due to the simple design, minimal maintenance and high efficiency. Some ventilation companies, such as JKF-Industries in Hadsund, Denmark, has been known to use a cyclone separator in series with a air bag filter, in order to remove the majority of the larger particles from the air, and thus limiting the maintenance needed for the bag filter. According to JKF-Industries, their cyclone separators, used in the wood processing industry, can often reach a solid loading of 100-300g/m^3, while the air bag filter often has a solid loading around 10g/m^3[7].

The two particle filtering technologies compliments each other well, with the cyclone being an easy and cheap method to remove the majority of the large particles and the bag filter removing the fine particles. It could be preferable to only use one technology and investigate the possibly of replacing a bag filter with one or more cyclones.

This could have the interest of JKF-Industries, that could benefit form this. One main issue with developing and testing new cyclones are that it can be difficult to determine the size of the particles that are put into the cyclone as well as the particles that escape capture. For this a CFD study could prove advantageous for the design and testing of various cyclones. Furthermore, a large interest point for JKF-Industries is the maintenance required for cyclones, which is considerably less than that of the bag filters that are primarily used by JKF-Industries.

2 Problem Analysis

This chapter will cover various methods of particle filtration, as well as why it is necessary to remove small particles from the air.

2.1 Particle Pollution in Air

Particles i the air can come from many places and have many different sizes. There are often differentiated between Particle Matter(PM) below 10 μm ,PM$_{10}$, and below 2.5 μm, PM$_{2.5}$. This is the size interval for the majority of airborne particles. Particles larger then 10 μm are not considered to be as harmful since they typically are captured in the nasal or throat area and does therefore not reach the lungs [25]. The size of the particle are generally given as the aerodynamic diameter. This is the equivalent diameter of a sphere with a density of 1000 kg/m^3 with the same terminal velocity [37].

The PM$_{10}$ are often deposited in the upper part of the lungs and in the larger airways, while the PM$_{2.5}$ travel deeper into the lungs and can pass into the bloodstream. It is primarily the PM$_{2.5}$ that is considered to contribute to lung cancer and heart disease [37]. The long term effect of PM$_{10}$ exposure are not totally clear but studies made by The International Agency for Research on Cancer (IARC) [19] did find an association between highly particle polluted areas and lung cancer. The estimated number of deaths linked to particle pollution every year is in the range from approximately 3-9 million people. A team from NASA estimated the number to 2.9 million and found that roughly 66% of the death occurring in China and India, two of the most polluted countries in the world. It is, however, not agreed as to how big a part of this, can be contributed to human made pollution or natural caused pollution [37]. Many of the PM$_{2.5}$ emitted by humans to the air are from sources such as combustion, wood processing and other industrial processes, while the natural air pollution often come from wind carried dust from e.g. deserts [37].

A task group on lung dynamics investigated the fraction of particles that are deposit in the lungs as a function of particle diameter and their finding can be seen in Figure 2.1 [9].
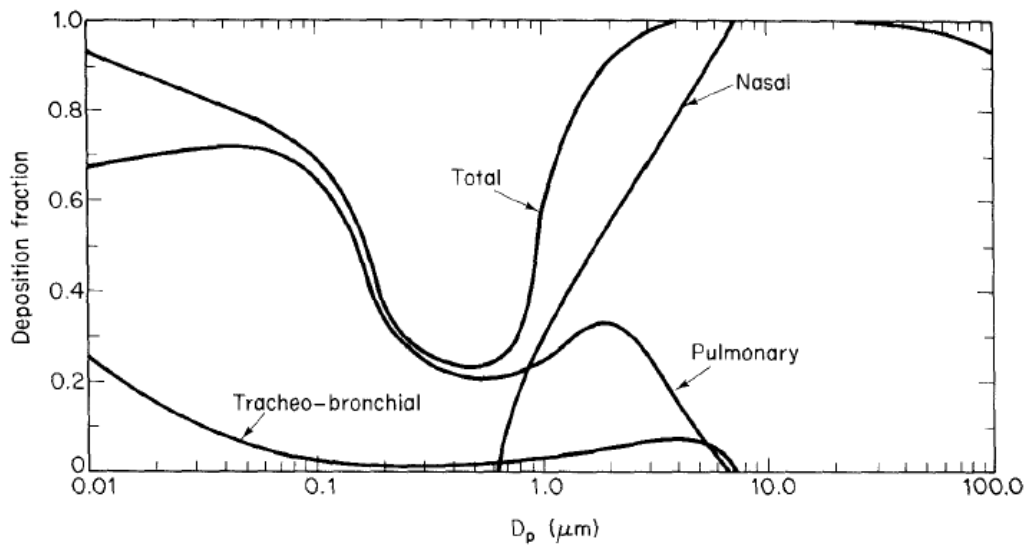
Figure 2.1: Deposition of aerosol particles in lungs with 15 respirations per minute and a tidal volume of 1450 cm^3. Figure from Flagan and Seinfeld [9].

It can be seen from Figure 2.1 that particles above the size of 10 μm are caught in the nose while most particles below one 1 μm passes through the nose. A large part of the particles below 0.1 μm are deposited in the lungs, but there seem to be a window between 0.1-1 μm where a large part of the inhaled particles are not deposited and escape through exhalation. The deposition curve is affected by the breathing volume, and respiratory rate, but does show that filtration of particles below 10 μm is necessary.

2.2 Particle Filtration Technologies

Filtration of particles from air can be done in several different ways. Three common methods are cyclone separators, wet scrubbers and cloth filters, all of which are well suited for various working conditions and particle sizes. On Figure 2.2 a comparison of which diameter ranges are most appropriate for the different technologies. The figure also shows typical diameter ranges of different substances.
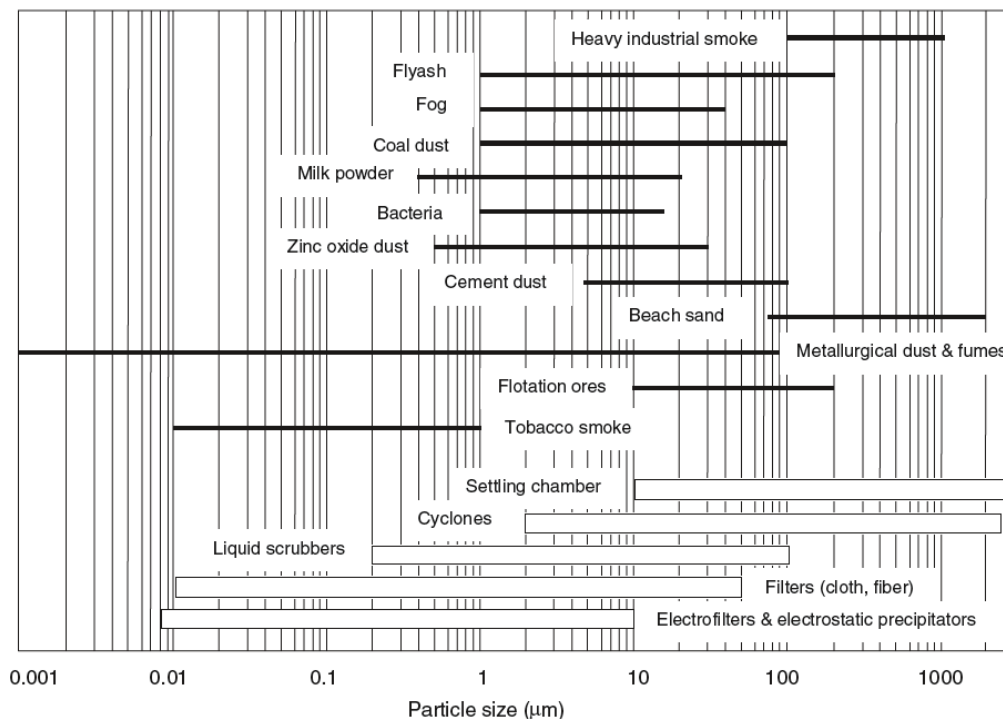
4

Figure 2.2: Overview of particle diameter separation ranges for different technologies and substances [15].

Settling champers are mostly used for particles larger than 10 μm where the particles can be separated with the force of gravity, for example, by slowing the air stream. However, for particles smaller than this, cyclones or cloth filters are often used in the production industry to separate particles from air.

It can be seen from Figure 2.2 that cyclones can typically be used down to 2 μm while cloth filters can be used down to 0.01 μm. The cloth filters has a high efficiency but can build up dirt and dust on the cloth which increases the pressure loss across the filter. The pressure loss across a cloth filter are therefore varying, which can be problematic in a ventilation system. This dirt has to be removed occasionally, leading to a temporary halt in filtration. The cloth filters also has some maintenance when the filterbags gets worn and need replacement [15].
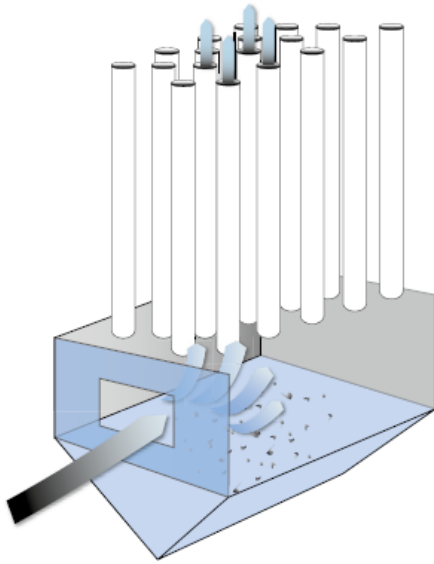
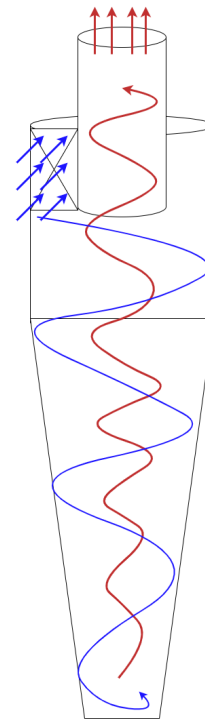**Figure 2.3:** Cloth bag filter [7].

Figure 2.4: High Efficiency Stairmand cyclone.

The main advantage of a cyclone is the production and maintenance cost, due to the fact that it can be produced from many different materials, depending on the intended purpose. Furthermore, a cyclone does not occupy much floor space, compared to a filter where the global velocity through the bag filters often needs to be slowed down significantly [7]. A cyclone can also be used under extreme working conditions, such as high temperature, pressure or when filtering chemically aggressive feeds [15].

A cyclone separator has a near constant pressure loss during operation, which generally tends to be higher than that of cloth filters.

One of the disadvantages of a cyclone is that it generally has a low separation efficiency below its designed cut size, which is defined as the particle size where the particle has a 50% chance of being captured. This cut size changes with varying volumetric flow, which can be a problem if incorporated into a dynamic system. In Figure 2.2 the cyclones are showed to have a range down to 2 μm, however this is very dependent on the size of the cyclone and this is rarely achieved on an industrial scale filtering by cyclones alone.

Due to the advantages of the cyclone, and that it in many cases is used to separate the coarse particles out of the air stream before entering a cloth filter, it is decided to investigate cyclone separation efficiency on smaller particles.

2.3 Cyclones

A cyclone separator works by sending air with particles into a cylinder in the tangential direction where the air will start to swirl towards the bottom of the cyclone. Due to the centrifugal force and the difference in density between the air and particles, the particles are pushed to the cyclone wall. At the bottom of the cyclone the air stream turns and creates a vortex core traveling towards the exit of the vortex finder pipe. The large particles will continue down and exit through the bottom of the cyclone while some of the smaller particles will follow the air stream through the vortex core and exit the cyclone. This is illustrated in Figure 2.5.

There are many different cyclone designs and geometries with varying parameters such as diameter, cone length, inlet and exit area. Where the cut size is very dependent on the tangential velocity which depend on the cyclone diameter. The pressure loss is of course also very dependent on the velocities, but geometric parameters such as cone length together with inlet and outlet conditions are also important parameters.

2.3.1 Stairmand Cyclone

The High Efficiency Stairmand cyclone is a proven and well tested cyclone developed by J.C Stairmand in 1951. The cyclone is widely used and are often taken as the basis for many studies and optimization tasks since it is a very well performing cyclone that can be scaled to many purposes. The design measurements of the cyclone are made in terms of the cyclone body diameter. This can be seen in Figure 2.5.
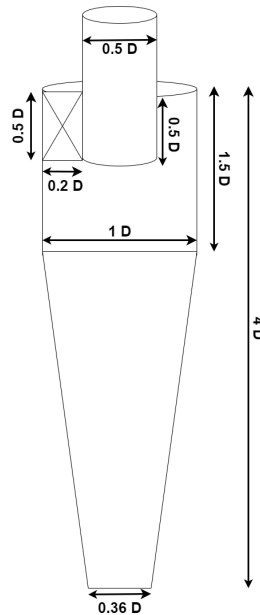

Figure 2.5: High Efficiency Stairmand cyclone with scalable dimensions.

The Stairmand cyclone will also be the basis design for this project. One of the upsides of this cyclone is that it is performing well for many applications and inlet velocities. However, it is unlikely that it is the optimal

design for both pressure loss and separation efficiency for a given system.

2.3.2 Separation Efficiency

The main issue with a cyclone separator is dependence between the separation efficiency and the particle size, where most modern cyclones are capable of filtering out particles of a size down to 10 μm. For particle sizes below 10 μm, the separation efficiency typically decreases considerably. One idea to increase the overall separation efficiency is to put multiple cyclones in series. This increases the probability to capture the small particles that escape the first cyclone. If considering a cyclone series of two, the cut size of the cyclones could also vary so that the first cyclone focus on separating the coarse particles and the second cyclone be a smaller cyclone to get a higher separation efficiency of the smaller particles.

A study was made by Venkatesh et al. [34], which showed that the comparison between a single cyclone and four cyclones in series, and how this affected the separation efficiency. The results and setup is shown in figure 2.6 and 2.7 respectively.
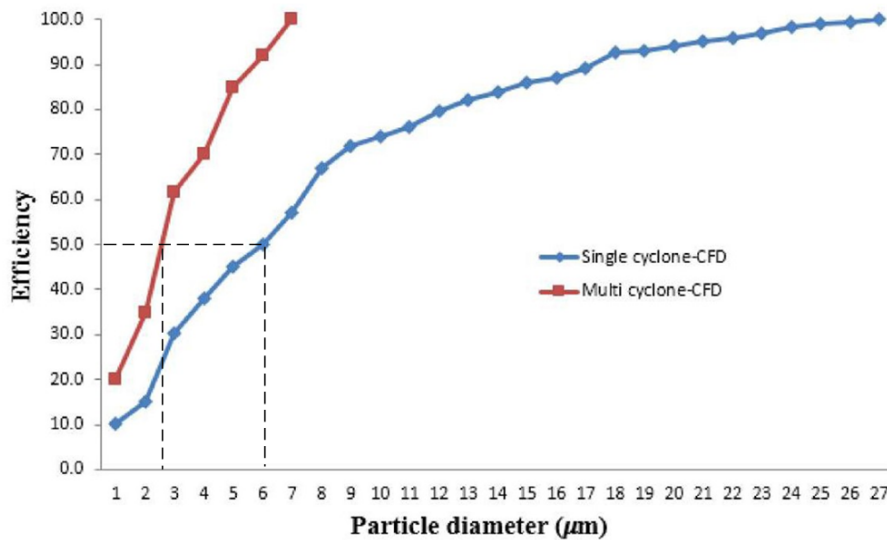

Figure 2.6: Separation efficiency of particles of different diameters for a single cyclone vs multiple cyclones in series. A dotted line has been added to illustrate the cut size, for both a single cyclone and several cyclones in series.
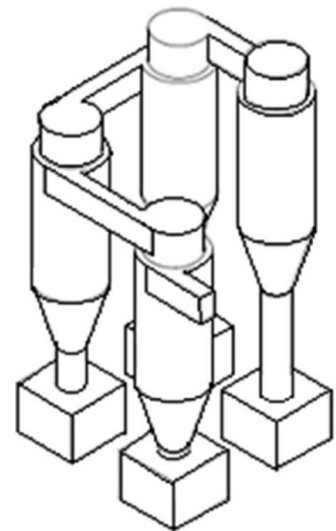
Figure 2.7: Multi cyclones in series.

From Figure 2.6 it can be seen that by putting four cyclones of the same size in series the separation efficiency is greatly increased and the cut size of the system is decreased from roughly 6 to 2.5 μm, shown by the dotted line. Therefore these multi cyclones could be an option to replace a bag filter.

The separation efficiency, $\eta(x)$, is defined as the number of particles, of a given diameter (x), that are trapped in the cyclone, or cyclone system, divided by the number of particles that enter the system of the given diameter.

The purpose of a cyclone is of course to have as high separation efficiency as possible but this often comes with the cost of increased pressure loss. Therefore it is also important to investigate how this can be limited.

2.3.3 Pressure Loss

The pressure loss that occurs in a cyclone is dependent on several factors like roughness, particle flow, geometry, etc. An increase in roughness of the inside of a cyclone separator will actually lead to a decrease in pressure loss in the cyclone [15].

Furthermore, it was shown by Tan, Karagoz, and Avci [33] that an increase in cyclone height generally leads to a decrease in pressure loss. It was also found that an increase in the diameter of the vortex finder lead to an decrease in pressure loss. The same is true when changing the diameter of the cone bottom of the cyclone. Another thing that can have an impact on the cyclone pressure loss and efficiency is the outlet design. This is something that can be added on the cyclone without changing the overall geometry, making it possible to incorporate on already operating cyclones without the need to produce a new cyclone.

Outlet Design

One of the things that could influence the performance of the cyclone is backflow from the outlet of the cyclone and back into the cyclone. The vortex in the middle of the cyclone exit along the wall of the vortex finder while backflow then can occur down the middle of the pipe. This is illustrated on Figure 2.8.
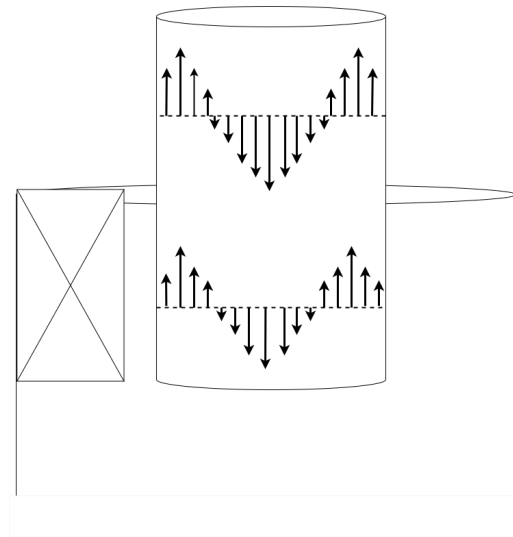

Figure 2.8: Illustration of backflow in the vortex finder.

Backflow has been reported in several papers. Boysan, Ayers, and Swithenbank [2] reported backflow in a High Efficiency Stairmand cyclone with a diameter of the backflow being half the vortex finder, extending all the way to the bottom of the cyclone. Measurements made on a Kahlsruhe cyclone with a 90°bend at the exit of the vortex finder showed to prevent backflow [13].

A study made by Souza, Vasconcelos Salvo, and Moro Martins [28], investigating the effect of a bend outlet pipe, and how the distance from the cyclone to the bend, as well as the bend radius, affects the pressure loss of a cyclone separator. This is shown in Figure 2.9.
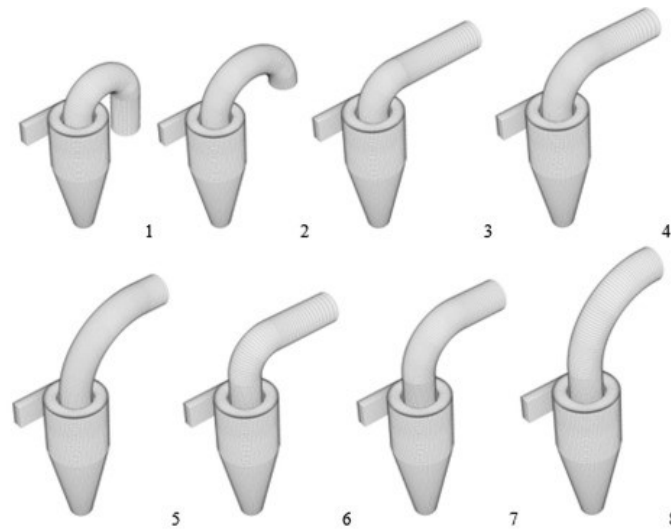
Figure 2.9: Cyclone outlet bends investigated by Souza, Vasconcelos Salvo, and Moro Martins [28].

Furthermore it was investigated how the outlet length of the cyclone affected the separation efficiency as well as the pressure loss. It was shown that an increase in the bend radius led to an increase in pressure loss for all outlet types and that a larger distance between the outlet and the bend led to an decrease in pressure loss and an increase in cut-size. The report does however not mention backflow or how these changes affected it. Funk [10] investigated the effect that evasés has on the pressure loss of a industrial size cyclone separator by testing rectangular and radial evasés, as shown in Figure 2.10
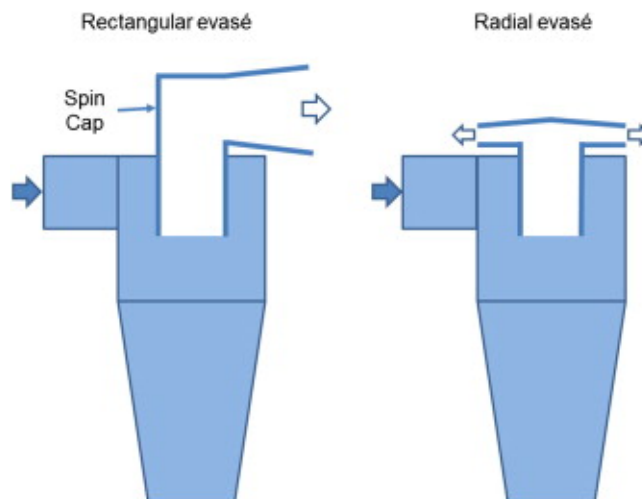

Figure 2.10: An illustration of the evasés tested by Funk [10].

Little to no change in pressure loss was measured when applying the rectangular evasé, but there was a slight decrease in the pressure losses when applying the radial evasés to the cyclone separator at increasing inlet velocities.

It was shown by Cao et al. [3] that a deswirler in the outlet of a cyclone separator can lead to a decrease in the

pressure loss, it does, however, also lead to a decrease in overall efficiency. The overall efficiency is defined as the ratio of particles captured to particles injected. Cao et al. [3] also showed that a hollow deswirler led to a decrease in the pressure loss, and also made an increase in overall separation efficiency. The results can be seen in Figure 2.11
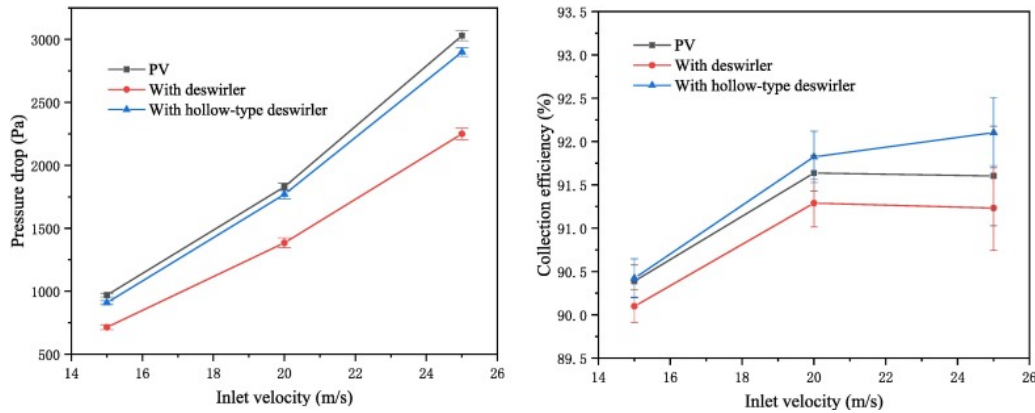

Figure 2.11: Results from Cao et al. [3]. PV is the regular cyclone type used to compare with different types of deswirlers.

Based on the observations made in problem analysis, it was decided that the main focus of this project is to investigate how various workloads, and cyclone design parameters, affects the backflow, pressure loss and separation efficiency. Furthermore, it will be investigated how this can be used to optimize a filtration system relying on multi cyclones.

3 Problem Statement

This leads us to the following problem statement:

> **How can various workloads, and design parameters, affect the performance of a filtration system relying on High Efficiency Stairmand Cyclones?**

To investigate this, the following subsidiary questions will be investigated using Computational Fluid Dynamics (CFD).

Subsidiary questions

- How does the inlet velocity affect the backflow and ultimately how does this affect the cyclone separation efficiency and pressure loss?

- How does a bend at the outlet affect backflow, pressure loss and separation efficiency of a cyclone separator?

- How can a a system of cyclones in series and parallel be used to optimize the separation efficiency and pressure loss compared to a single cyclone separator.

Problem Definition

This project will mainly consider the High Efficiency Stairmand cyclone. This is a well documented and tested cyclone that work well for many applications. The Stairmand cyclone is by many considered to be a standard cyclone design and many experimental tests and optimization tasks has been performed on this cyclone. It has been found that the cyclone design in some conditions can suffer from a phenomenon called "presessing vortex core". This is where the vortex core gets close to the cyclone wall, which can negatively impact the separation efficiency [41]. The cyclone is considered to be a good starting point for investigation into cyclone behavior and is mainly chosen due to its simplistic design and available experimental data.

Limitations

The following factors will not be taken into account for this project.

- The project does not include any experiments, but relies on the experimental data of others to validate models and simulations.

- It is assumed that the solid loading is sufficiently low so that particle-particle interaction and interaction with the continues phase is assumed negligible.

- All simulations in this project assumes a constant workload, with no change in volumetric flow.

4 Theoretical Pressure and Efficiency

This chapter will cover how the pressure loss can be calculated using methods originally presented by Stairmand, as well as the efficiency and cut size using the Muschelknautz methods. Additionally this chapter will cover the main principles in scaling of cyclone separators, as well as the relevant theory for particle laden flows.

4.1 Scaling of Cyclone

When designing a cyclone it can be advantageous to make a geometrically similar, scaled down cyclone, in order to predict the performance of a full scale cyclone. The model scaling can, with some simple assumptions, in many cases predict the performance of a prototype cyclone more accurately than mathematical models for pressure and performance. When scaling a cyclone the values of interest are often the cut size and the pressure loss of the cyclone [15]. For this project a scaling of the Stairmand cyclone with an internal diameter of 290 mm will be used. This is chosen due to available experimental data on this cyclone at that size and will later be used to validate the models.

To scale the cyclone a dimensionless analysis with some assumptions will be used. First an analysis of the physical and operational parameters influencing the separation efficiency will be made. Some of the things that influence the separation efficiency is the cyclone body diameter D, the dynamic viscosity μ and density ρ of the fluid, the density difference between the densities of the particle and fluid $\Delta\rho$, the particle size x and the characteristic velocity of the cyclone v_{ch} taken as the inlet velocity.

$$\eta(x) = f(D, \mu, \rho, \Delta\rho, x, v_{ch}) \tag{4.1}$$

Some of the criteria and assumptions made are that the scaled geometrically with the same measurement ratios. It is also assumed that the particles always are at their terminal velocity and that the solid mass loading is light (<3 grams pr kilo air), so the particles influence on the airflow can then be neglected. At light loading the effect of gravity can also be ignored due to the assumption that the centrifugal force is the acting dominant force. The effect of relative roughness of the cyclone walls are also neglected and is thereby ignoring the difference in relative roughness between a model and a prototype [15].

By using the dimensionless analysis Buckingham pi theorem, the parameters can be split up into different dimensionless parameters.

$$\eta(x) = f\left(\frac{D\rho v_{ch}}{\mu}, \frac{x}{D}, \frac{\Delta\rho}{\rho}\right) \tag{4.2}$$

The first term can here be recognized as the Reynolds number which describe the flow pattern. By rearranging the dimensionless parameters the Stokes number will arise, which describe the particles movement in the

flow.

$$Stk = \frac{1}{18} \cdot \frac{D\rho v_{ch}}{\mu} \cdot \frac{\Delta\rho}{\rho} \cdot \left(\frac{x}{D}\right)^2 \tag{4.3}$$

Since all of the terms are included in the Stokes number it can replace any of the dependent terms. It will therefore replace the second term. Furthermore, by analysing the equation of motion for particle flow Hoffmann and Stein [15] showed that the density ratio is not needed to be a term of its own when included in the Stokes number. This leads to the separation efficiency being a function of only Reynolds number and Stokes number. In many cases the designer of the cyclone is only interested in the cut size. This will be where $\eta(x) = 0.5$.

Since it is only the Stokes number that is a function of particle size x, then we can write the cut size stokes number as Stk_{50}.

$$Stk_{50} = f(\text{Re}) \tag{4.4}$$

If the model is much smaller than the prototype, it can be difficult to maintain the same Reynolds number without requiring very high velocities. To compensate for this the fluid could be changed to water, however this also has its own challenges when it comes to particle dispersion. For example incomplete surface wetting or swelling [15].

Overcamp and Scarlett [26] investigated the influence of Reynolds number on the Stk_{50} and found that there was a weak dependence. From Reynolds numbers above $2 \cdot 10^4$ the Stk_{50} is almost independent of the Reynolds number. This can be seen in Figure 4.1, where a plot of the Stk_{50} is plotted as a function of Reynolds number for a variety of different cyclones.
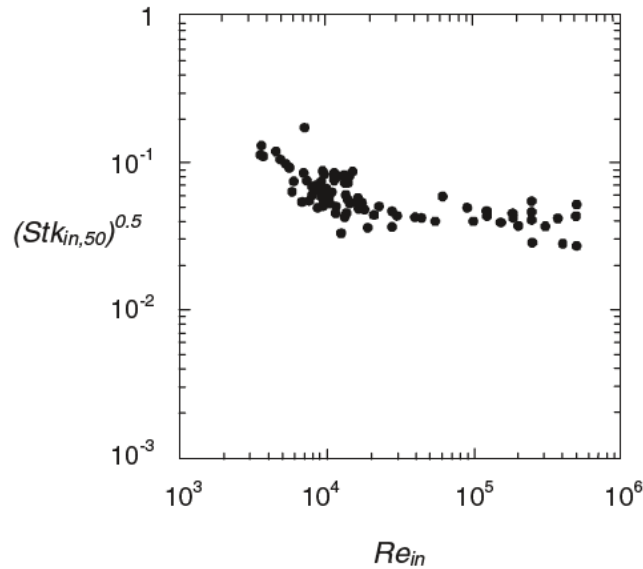

Figure 4.1: Stk_{50} as a function of inlet Reynolds number for a range of different cyclones. Figure from Overcamp and Scarlett [26]

Since most commercial cyclone are operated in the range of $10^5 - 10^6$ it is in most cases sufficient to consider the Stokes scaling.

The same practice as for the cut size can be made for the pressure loss over the cyclone using some of the same assumptions then the pressure loss can be written as a function of density, viscosity, velocity and diameter.

$$\Delta p = f(\rho, \mu, v_{ch}, D) \tag{4.5}$$

This can be written with dimensionless parameters as:

$$\frac{\Delta p}{\rho v_{ch}^2} = f\left(\frac{D\rho v_{ch}}{\mu}\right) \tag{4.6}$$

Here the pressure term on the left side of the equation is half the Euler number, which is given as the ratio of pressure loss to dynamic pressure. The right side of the equation can again be recognised as the Reynolds number.

$$Eu = f(\text{Re}) \tag{4.7}$$

There is again a weak dependence between the Euler number and Reynolds number at high Reynolds numbers. This is partly due to the friction factor being nearly independent of Reynolds number in fully turbulent flow. However there is some dependence on the Reynolds number which could cause an over prediction in pressure loss if a small model is scaled to a large prototype only by considering Euler scaling.
To find the pressure loss in Euler scaling the same pressure loss equation as for other flow devices such as pipes and bends can be used, seen in equation 4.8.

$$\Delta p = k \cdot \frac{1}{2}\rho v_{ch}^2 \tag{4.8}$$

Here k is the Euler number for the model. Before using the these scaling laws, one should consider if it is applicable in the given situation and within the bounds of the assumptions.

4.2 Pressure Loss

The velocity distribution in the cyclone can be calculated from a moment of momentum balance, and then used to estimate the pressure loss as entrance losses, exit losses and loss of static pressure in the swirl.
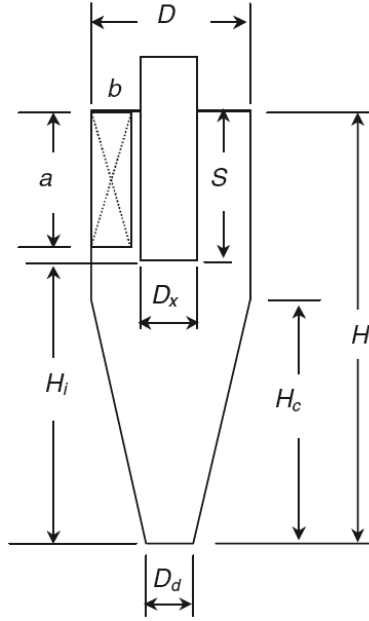
Figure 4.2: Symbolic measurements of the cyclone used in this section.

The total pressure loss in a cyclone can be calculated as shown in equation 4.9. This method was first presented by Stairmand and later worked out in a compact form by Iozia and Leith [17].

$$\frac{\Delta p}{\frac{1}{2}\rho v_{in}^2} = Eu = 1 + 2q^2\left(\frac{2(D-b)}{D_x} - 1\right) + 2\left(\frac{4ab}{\pi D_x^2}\right)^2 \tag{4.9}$$

Where v_{in} is the inlet velocity and q is a calculated value found as shown in equation 4.10

$$q = \frac{-\left(\frac{D_x}{2(D-b)}\right)^{0.5} + \left(\frac{D_x}{2(D-b)} + \frac{2A_R f}{ab}\right)^{0.5}}{\frac{A_R f}{ab}} \tag{4.10}$$

Where A_R is the total surface area of the cyclone wall, including the inner walls of the lid as well as the outer wall of the cyclone finder. The wall friction factor f is set to 0.005 for high Reynolds numbers which under normal conditions apply to cyclones [15]. This is the friction factor for air in a hydraulic smooth cyclone, which at low relative roughness is a fair number. If particles are present, the friction factor will increase due to the slow moving particles on the cyclone wall increasing the roughness. The total friction factor therefore becomes dependent on the mass loading. The total friction factor can be found as [15]:

$$f = f_{wall} + f_{particles} = f_{wall} + 0.015\sqrt{\dot{m}_p}) \tag{4.11}$$

The friction factor of the particles at a solid loading of 10 g/m^3 is approximately 27% higher then that of a smooth wall. Even though the friction factor increases, the overall pressure loss decreases. This is because the increase in wall roughness and drag between the particles and air slows the tangential velocity down. This

also decreases the swirl in the core vortex. Since much of the dynamic pressure is stored in the swirl and most of this is lost in the vortex finder and downstream piping, a reduction in swirl will decrease the overall pressure loss. It is however not desirable to increase the roughness of the cyclone walls, since a decrease in tangential velocity also will decrease the separation velocity.

4.2.1 Comparison With Experimental Results

By comparing the results gathered using the equations presented in this section, to the experimental results presented by Hoekstra [14] it was found that there was a average deviation in the pressure equal to 40.6Pa with the highest and lowest deviation being 77.3 and 11.3Pa respectively. A comparison can be seen in figure 4.3. The experiment was conducted without particles and mathematical calculations was made with a friction factor of 0.005.
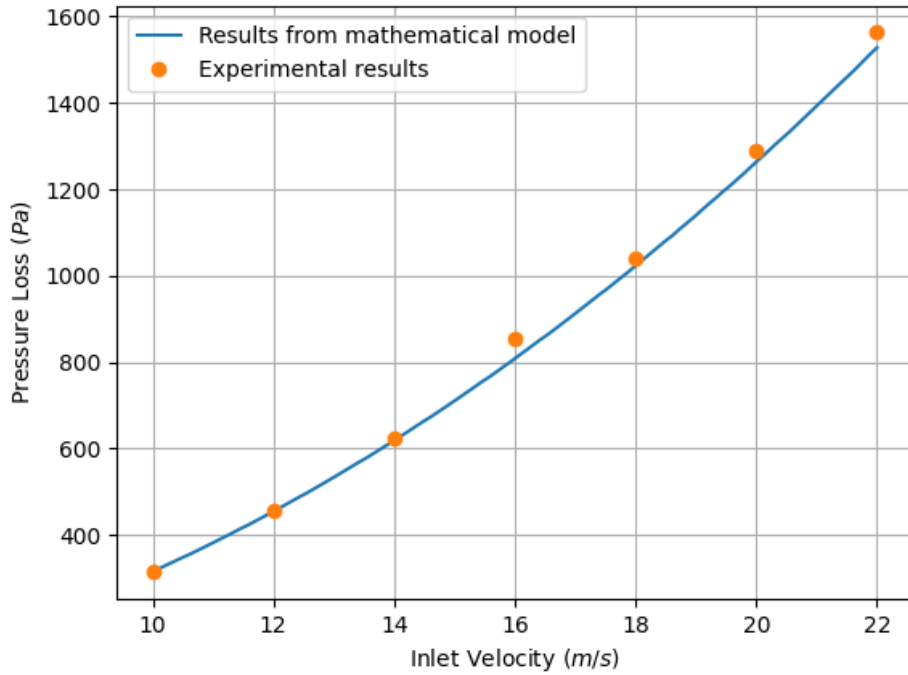

Figure 4.3: A comparison of the calculated pressure loss and the experimental pressure loss presented in Sun et al. [30] on a Stairmand cyclone with a diameter of 290 mm.

From the results in Figure 4.3 it can be seen that the mathematical model makes a fairly precise estimate of the pressure loss in the cyclone.

From Figure 4.3 the experimental data can be fitted to a second-order polynomial function with a $R^2 = 0.9995$. The equation can be seen in Equation 4.12.

$$\Delta p = 3.2 \cdot v^2 - 3.1 \cdot v \qquad (4.12)$$

The value 3.2 in Equation 4.12 can be seen as the $\frac{1}{2}\rho Eu$ in Equation 4.8. This makes the Euler number of the cyclone ≈ 5.3. It can also be seen that there is a negative first-order term which show that the Euler number is in fact not constant, but has some Reynolds number dependency. This means that for higher Reynolds numbers, the Euler number decreases. Hoffmann and Stein [15] estimated this Reynolds number dependency on the Euler number to be to the power of -0.17 to -0.2.

4.3   Efficiency and Cut Size

The separation efficiency is used to estimate how many particles of a specific diameter is captured by the cyclone, while the cut size is the specific particle size where 50% of the particles are captured by the cyclone. Both of these can be calculated using Muschelknautz Method, presented in Hoffmann and Stein [15].
The cut size is found as shown in equation 4.13

$$x_{50} = x_{fact}\sqrt{\frac{18\mu(0.9Q)}{2\pi(\rho_p - \rho)v_{\theta CS}^2(H - S)}} \tag{4.13}$$

Where x_{fact} is a correction factor that is used to fit the cut size to experimental results. Q is the volumetric flow rate that can be seen to be multiplied by 0.9, this is due to the estimation of that 10 % of the flow "short circuit" and flow directly from the top of the cyclone and into the vortex finder. ρ_p and ρ is the density of the particles and air respectively and $v_{\theta CS}$ is the tangential velocity of the air at the inner core radius.
Using this, the separation efficiency at various diameters can be found as shown in equation 4.14

$$\eta_i = \frac{1}{1 + \left(\frac{x_{50}}{x_i}\right)^m} \tag{4.14}$$

where x_i is the diameter of a single particle, and m is a factor determining the steepness of the slope for the efficiency curve.
m can vary from 2 to 7 and is found by comparing the calculated slope with experimental results, and choosing the value that yields the most accurate results. If this is not possible the value can be chosen based on a cyclone with similar design and working conditions. For smooth walled cyclones m is often between 4 and 6.
The cyclone efficiency curve, as well as the cut size at an inlet velocity of 16.34 m/s can be seen in figure 4.4.
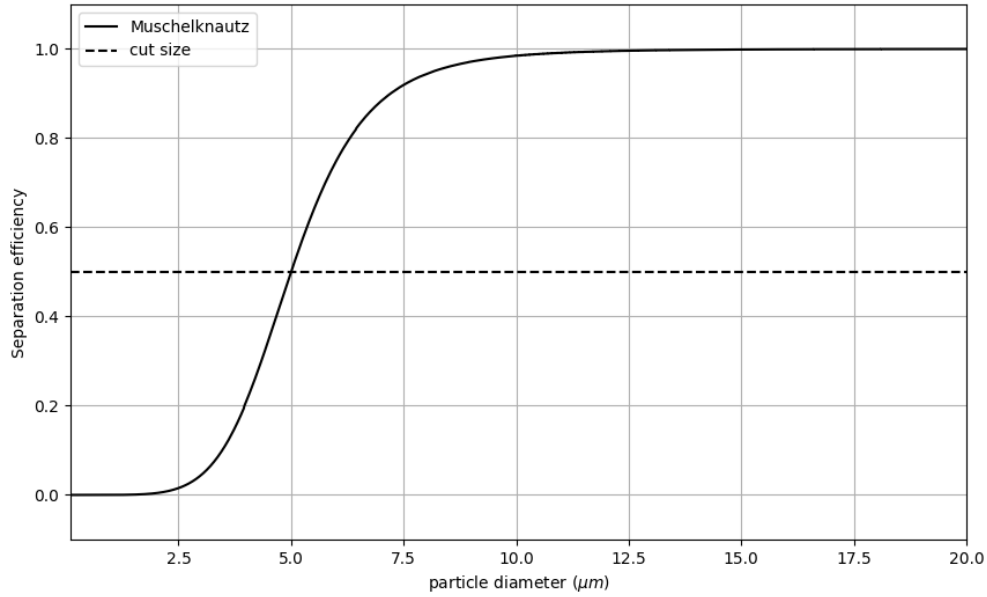
Figure 4.4: The separation efficiency depending on particle diameter.

The cut size for this cyclone was calculated to be $6.239 \mu m$. From the separation efficiency curve the overall efficiency can be calculated. This is defined as:

$$\eta_s = \frac{\text{Particles trapped}}{\text{Particles in}} \tag{4.15}$$

A lowering of the cut size therefore increases the overall efficiency for a given particle distribution.
Lowering the cut size usually also comes with the cost of pressure loss. This relation between the cut size and pressure loss should for reasonable cyclone designs according to Svarovsky [32] follow Equation 4.16.

$$Eu_a \sqrt{Stk_{a_{50}}} = \sqrt{12} \tag{4.16}$$

Here the variables are expressed as the dimensionless cut size Stk_{50} and Euler number. The subscript "a" indicate that the characteristic velocity of the Euler number and Stokes number has to be taken as the average axial velocity of the cyclone body.

4.4   Multiphase Flow

When solid particles are submerged in a gas-flow, such as air, it is characterised as multiphase flow. The air is carrying the particles with the flow and the motion of the particles in the air stream are influenced by a number of things. There are two different types of flows which are distinguished between, dilute and dense flow. These are characterised by the volumetric fraction.

$$\alpha_p = \frac{V_p}{V} \tag{4.17}$$

The flow is considered dilute if the volume fraction is below 10^{-3} and dense if above. In dense flow, the particle movement is primarily controlled by particle-particle collisions, whereas in dilute flow the particles can be treated as isolated and are controlled by aerodynamic forces.

Cyclones in the wood industry typically operate at a volume fraction below 10^{-3} [7]. For this project the flow is therefore assumed to be dilute in the cyclone.

4.4.1 Particle Motion

How close the particle will follow the airflow is described by the Stokes number. The Stokes number is defined as the ratio of the particle momentum response time τ_v to the characteristic time of the flow τ_f. Here the particle response time is the time for a particle released from rest to reach 63% of the free stream velocity.

$$Stk = \frac{\tau_v}{\tau_f} \tag{4.18}$$

$$\tau_v = \frac{\rho_p d_p^2}{18\mu} \tag{4.19} \qquad\qquad \tau_f = \frac{D_T}{U_T} \tag{4.20}$$

The characteristic time of the flow is determined by the free stream velocity U_T and the characteristic length of the flow D_T. For Stokes numbers much larger than unity the particle will separate from the flow in sudden accelerations, whereas for Stokes numbers much lower than unity the particle will follow the flow closely. This number is very relevant when considering scaling of cyclones.

To further analyse the motion of a submerged particle, the equation of motion in dilute flow can be used.

$$\rho_p V \frac{d\vec{v}}{dt} = \frac{1}{2}C_D \rho_f A_p |\vec{u} - \vec{v}|(\vec{u} - \vec{v}) + V(\rho_p - \rho_f)\vec{g} + \sum F_{other} \tag{4.21}$$

The different terms from the left in equation 4.21 are the inertia, drag, gravitational and other forces. The drag term in this equation is generally the dominating term on small particles. The gravity term primarily plays a role if the particles are large and heavy. The other forces that may be included in this equation are mostly minor forces, but may be of significance in certain situations, for instance where the density ratio between the particle and fluid is close to unity or when dealing with sub-micron particles. Since this project is dealing with airflow with solid particles where the particle density is much greater than the air density and the majority of the particles are larger then one micron these forces are considered negligible. Another force that becomes relevant when dealing with cyclones is the centrifugal force, which is greatly dependent on the particle diameter. The centrifugal force can be calculated as:

$$F_{centrifugal} = \rho_p \frac{4}{3}\pi \left(\frac{D_p}{2}\right)^3 \cdot \frac{v^2}{R} \tag{4.22}$$

The airflow is not only affecting the particle movement, but for particle volume fractions above 10^{-6} the particles influence on the airflow should also be taken into account. This is called two way coupling, and depending on the Stokes number the particle can either decay or enhance turbulence. With high stokes numbers enhancing turbulence and smaller Stokes numbers decaying turbulence.

4.4.2 Particle Shape

Since the motion of the particle is highly influenced by drag, the drag coefficient C_D is an important factor. The drag coefficient is a function of both shape and the particle Reynolds number. The particle Reynolds number is based on the slip velocity between the particle and the carrier phase.

$$Re = \frac{\rho_f |\vec{v}_f - \vec{v}_p| D_p}{\mu} \tag{4.23}$$

The particle Reynolds number is also dependent on the diameter which often varies according to a particle distribution. On Figure 4.5 the drag coefficient as a function of Reynolds number on a smooth sphere is graphed.
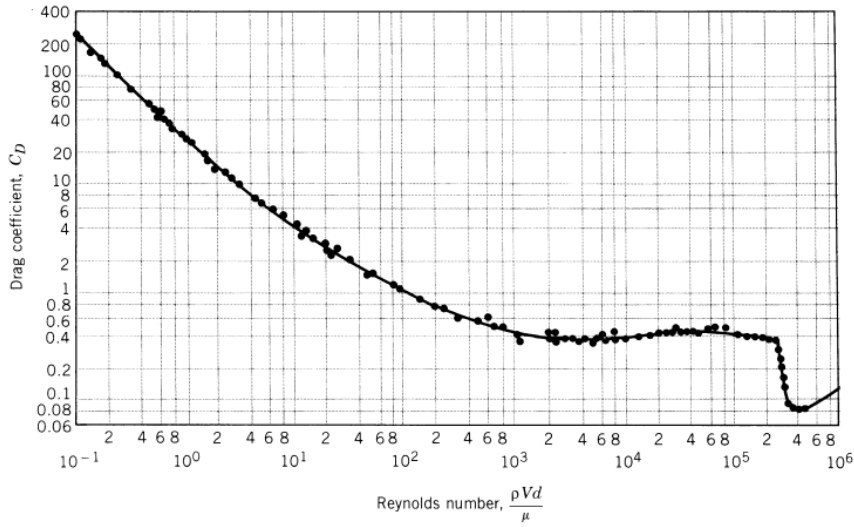

Figure 4.5: The drag coefficient of a smooth sphere as a function of Reynolds number. Figure from Cimbala [6]

The shape of the particle will be assumed as a smooth sphere since knowledge of the average particle shape is unknown and would require assumptions of its own. If the shape of the particles are known, a non-spherical shape factor can be included [1].

Furthermore for small particles with low Stokes number the particles will follow the flow closely and the Reynolds number will therefore be small. For Reynolds numbers in the Stokes flow regime (Re<1) the particle drag coefficient is in many cases nearly independent from both shape and roughness[11]. The drag

coefficient for a smooth sphere is calculated as:

$$C_D = a1 + \frac{a2}{Re} + \frac{a3}{Re^2} \tag{4.24}$$

The constants a1, a2 and a3 are determined by Morsi and Alexander [24] and are all stepwise functions of the Reynolds number [1]. The values of a1, a2 and a3 are shown in Table 4.1

Reynolds number	a1	a2	a3
0<Re<0.1	0	24	0
0.1<Re<1	3.69	22.73	0.09
1<Re<10	1.22	29.17	-3.89
10<Re<100	0.62	46.50	-116.67

Table 4.1: Values of a1, a2 and a3 at different ranges of Reynolds number [24].

5 CFD

This chapter will cover the core concepts of how CFD is used to simulate cyclone separators for this project. It will describe the various models and settings needed to simulate the flow and particle behavior properly. Furthermore this chapter contains a description of the mesh used, as well as a validation of the mesh and simulations.

5.1 Turbulence Model

A cyclone separators working process contains complicated three dimensional swirling, making the flow very complex, and simulation hereof relatively difficult. In order to predict the flow field characteristics of the swirling flow, using CFD, a proper turbulence model is necessary.

5.1.1 Governing Equations

In this project the Reynolds Average Navier Stokes (RANS) will be used. This uses the Reynolds decomposition of the velocity in the Navier Stokes equation to split the velocity into a time averaged and a fluctuating velocity. The RANS then only considers the time averaged value. This makes it a lot less computationally heavy then other models that takes the fluctuating velocity into account. The governing equations of the RANS model are the continuity and momentum equation seen in Equation 5.1 and 5.2.

$$\frac{\partial \rho}{\partial t} + \nabla \cdot (\rho \vec{v}) = 0 \tag{5.1}$$

$$\frac{\partial}{\partial t}(\rho \vec{v}) + \nabla \cdot (\rho \vec{v} \vec{v}) = -\nabla \vec{p} + \nabla \bar{\tau} + \rho \vec{g} + \vec{F} \tag{5.2}$$

Here τ is the stress tensor and F is a external force, which can be included in for example multi phase flow from interaction with a dispersed phase [1]. Since the RANS model does not in itself model the turbulent effects of the flow, a turbulence model is needed. Here the Reynolds Stress Model (RSM) and the Renormalised group (RNG) k_ϵ are both commonly used when simulating cyclone separators. [40]

5.1.2 Literature Study of Turbulence Model

According to Sun et al. [31] the RSM model gives a much more reasonable prediction for a strong swirling flow when compared to two equation models such as the $k - \epsilon$ variants, though it also requires additional computing resources, even though those are considered to be relatively limited.
According to Misiulia et al. [23] the RSM has been proven to be the most appropriate RANS turbulence model for the prediction of swirling flows.

A study was made by A Cen, Zhao, and Shen [5] showing how the RNG $k - \epsilon$ and the Omega RSM model have similar results when simulating flow fields and the variation of swirling intensity. The same is true for the general velocity field. The Omega RSM did give considerably better results when calculating the turbulent viscosity.

Hoffmann and Stein [15] also compared both first and second order accurate RNG $k - \epsilon$ and RSM models to experimental data of a velocity profile across a gas cyclone. This showed that a second order accurate model was necessary to capture some of the backflow in the cyclone. Both the RNG $k - \epsilon$ and RSM showed acceptable results.

To investigate which of the models are most appropriate for this project and simulation on this cyclone, a comparison of the two turbulence models will be made.

5.1.3 Reynolds Stress Model (RSM)

The Reynolds Stresses Model is the most elaborate turbulence model used when using RANS simulations. The RSM closes the Reynolds Average Navier Stokes Equations by solving the equations for the Reynolds stresses and the dissipation rate together. This leads to an additional seven transportation equations for a 3D simulation.

The main advantage of the RSM turbulence model is an improved performance in flows with a strong swirling component, flows with a sudden change in the mean strain rate, flows with a strong streamline curvature and finally an improved performance for flows with a strong secondary circulation.

The main disadvantage for such high flexibility in the RSM is a high complexity in the resulting mathematical system, that often lead to a decrease in numerical robustness and an increase in required computational power.

It is possible to increase the numerical stability of the RSM by starting with a more stable turbulence model, such as the RNG k-ϵ, followed by the RSM. The RSM might acquire more iteration before reaching convergence than the k-ϵ due to the strong coupling between the Reynolds stresses and the mean flow. [12]

5.1.4 Renormalized Group (RNG) k-ϵ

The RNG $k - \epsilon$ model is similar to the standard $k - \epsilon$ but includes an additional term in the ϵ equation that improves the accuracy for rapidly strained flows. The RNG model also includes the effects of swirl on turbulence, enhancing the accuracy for swirling flows.

The RNG $k - \epsilon$ is derived from the instantaneous Navier-Stokes equations, using the Renormalization group method, which results in a model with different constants than the standard $k - \epsilon$ as well as additional terms and functions in the transport equations for k and ϵ:

The RNG $k - \epsilon$ modifies the turbulent viscosity, to account for swirls in the flow. This modification takes the functional form shown in equation 5.3.

$$\mu_t = \mu_{t0} f \left(\alpha_s, \omega, \frac{k}{\epsilon} \right)$$

(5.3)

Where μ_{t0} is the turbulent viscosity calculated without the swirl modification, ω is a characteristic swirl number and α_s is a swirl constant that assumes different values depending on whether the flow is swirl dominated or only mildly swirling.

5.1.5 Comparison of Turbulence Models

The two turbulence models are compared to the experimental data from the Stairmand cyclone made by Hoekstra [14]. This experimental data is widely used for validation of the High Efficiency Stairmand cyclone. Here the axial and tangential velocity profile is measured in the cyclone body, 0.25D from the vortex finder.

(a) Normalised tangential velocity.

(b) Normalised axial velocity.
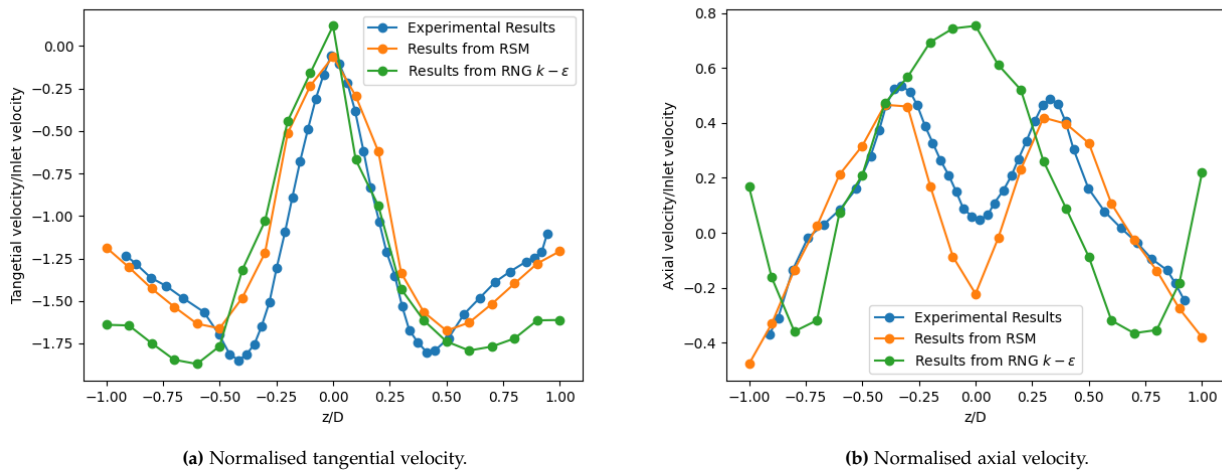
Figure 5.1: Comparison of RSM and RNG $k - \epsilon$ to the experimental results.

The simulations carried out on the two models are made with the settings described later in this chapter. It can be seen from Figure 5.1 that the RSM are more accurate on both velocity profiles. The RNG $k - \epsilon$ predicts the tangentiel velocity decently but have some overestimation of the swirl along the cyclone walls. On the axial velocity it completely misses the backflow in the middle of the cyclone. The RSM predicts the flow well except a slight overestimation on the backflow in the axial velocity profile.

Therefore the RSM turbulence model was chosen for this project.

5.2 CFD Model Choices

5.2.1 Scheme

For the pressure-velocity coupling, the Semi-Implicit Method for Pressure-Linked Equations (SIMPLE) scheme is used. This algorithm uses a guessed pressure field to solve the momentum equation. If the fluxes does not satisfy the continuity equation a flux correction is added and used to calculate a corrected pressure and velocity field. This is then iterated until a converged solution is obtained. [1].

5.2.2 Differencing Scheme

The Differencing scheme chosen for the simulations is a second order upwind scheme on the momentum, Reynolds stresses, turbulent kinetic- energy and dissipation rate. It was showed by Hoffmann and Stein [15] that a second order Reynolds stress model is preferable to a first order model for accurate results. In the second order upwind scheme, the cell face value ϕ_f is approximated as the upstream cell center value ϕ_{upwind} together with its gradient as seen in equation 5.4 [1].

$$\phi_f = \phi_{upwind} + \nabla \phi_{upwind} \cdot \vec{r} \tag{5.4}$$

Here the $\vec{r}$ it the displacement vector between the cell face and the upwind cell center. Furthermore the gradient is limited so that the face value remains within the value of the two cells.

The pressure differencing scheme is chosen as the PREsure STaggering Option (PRESTO), which is recommended for strongly curved domains and flow with high swirl. The PRESTO scheme uses a staggered control volume grid approach to calculate the pressure at the cell face and can be applied to all meshes [1].

5.2.3 Boundary Conditions

The inlet conditions are set as a plug flow with a defined velocity. Due to the unknown upstream conditions and a fully turbulent velocity profile being relatively flat, the plug flow seems as a reasonable assumption [13]. The turbulent intensity is assumed to that of a fully developed pipe flow and can be calculated as a function of the Reynolds number in equation 5.5

$$I = \frac{v'}{v_{avg}} = 0.16 \cdot Re_{D_h}^{-1/8} \tag{5.5}$$

With a average velocity of 16.34 m/s this results in an intensity of approximately 4%. The outlet conditions are set to atmospheric pressure.

For the discrete phase model, the particles are set to reflect in a perfectly elastic collision with the cyclone walls. In the bin at the bottom of the cyclone the walls are set to trap the particles.

5.2.4 Wall Function

Standard wall function

For the standard wall function the law of the wall for mean velocity fields can be seen in equation 5.6

$$u^* = \frac{1}{k} ln(Ey^*) \tag{5.6}$$

Where $k = 0.4187$ is the von Karman Constant, $E = 9.793$ is an empirical constant The dimensionless velocity U^* is based on the the dimensionless distance from the wall y^*. This is similar to the dimensionless distance y^+, but differ in the way the dimentionless scale is calculated. Where y^* is based on the turbulent kinetic

energy and y^+ is based on the wall shear stress. For most flows the two approaches have similar results [39]. y^* is expressed as

$$y^* \equiv \frac{\rho C_\mu^{1/4} k_P^{1/2} y_P}{\mu}$$ (5.7)

Here k_P is the turbulent kinetic energy of the near wall node P and y_P is the distance from point P to the wall.

The logarithmic law for mean velocity is considered valid for $30 < y^* < 300$ but is employed in Ansys when $y^* > 11.225$. When $y^* < 11.225$ the linear relationship between u^* and y^* is used.

$$u^* = y^*$$ (5.8)

The point where $y^* = 11.225$ is the intersection of the linear and log law. This makes the standard wall function a two layer model with no blending of the two functions in the transition buffer layer where the error is the highest. This can be seen in Figure 5.2. The red line being the Spalding boundary layer equation [29]. This is a continuous equation that describe the boundary layer accurately between a y^* of 0 to 300.
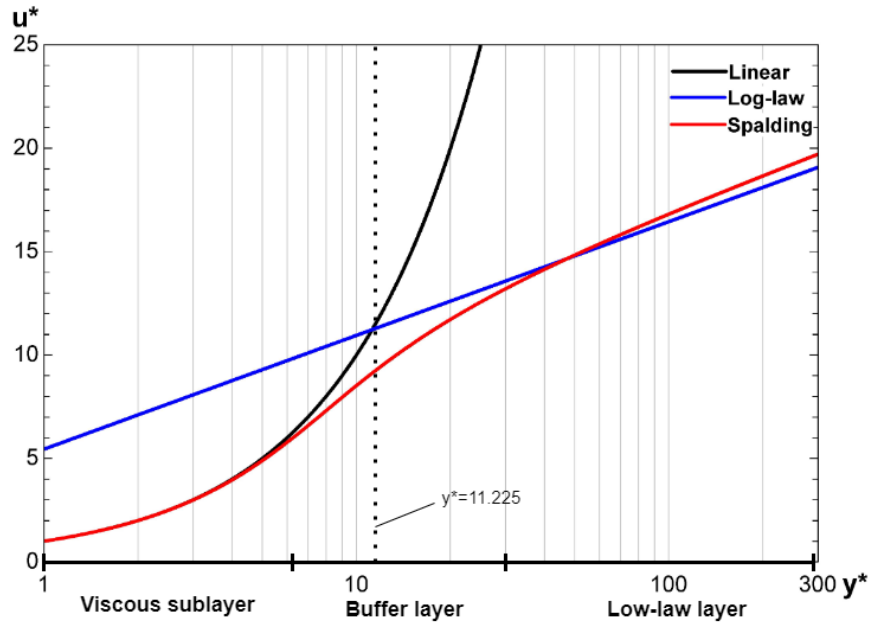
Figure 5.2: Dimentionless boundery layer velocity profile.

In the standard wall function the first cell center should be located in the log-law layer to ensure accurate results. This can however be a difficult task to ensure, especially in domains with varying wall refinements or flow conditions.

Scalable Wall Function

The main concept of the scalable wall function is keeping the value of y^* above 11.225 in order to force the use of the log-law in the first cell from the wall.[22].

This is done by introducing a limiter in the y^* calculations:

$$y^* = MAX(y^*, y^*_{limit}) \tag{5.9}$$

where $y^*_{limit} = 11.225$

This replaces all instances of y^* in the standard wall function with the same of the scalable wall function.

If $y^* > 11.225$, the scalable wall function is identical to that of the standard wall function. [22]

With varying velocities on the cyclone walls, the scalable wall function is therefore used in this project.

5.3   Discrete Phase Model

The particle trajectories are modelled using a Discrete Phase Model (DPM) which is based on the Euler Lagrange approach. Where the flow field is calculated with the Navier Stokes equations and the dispersed phase is solved by tracking a large number of particles through the calculated flow field. One assumption in the DPM model is that the particle-particle collisions and the volume loading is small and can be neglected [1]. In these cases of fine dust particles, the volume fractions are below 10^{-6}. This means that one way coupling is a fair assumption and the particles turbulence effect on the carrier phase can be neglected [21].

To model the random effects of turbulence on the particles, the discrete random walk model is used. The particle trajectory is predicted using the mean fluid velocity $\bar{v}$ together with a instantaneous fluctuating velocity v'.

$$v = \bar{v} + v' \tag{5.10}$$

The instantaneous fluctuating velocity is determined using the random walk model. In this model the fluctuating velocity is kept constant over a characteristic eddy lifetime. The eddy lifetime is approximated as:

$$\tau_e \approx -0.3 \frac{k}{\epsilon} \cdot ln(r) \tag{5.11}$$

Where r is a random number between 0 and 1 [1]. This generates a randomness to the eddy lifetime. The trajectory of a particle is then computed in a set "number of tries" where each try has its own streamline. With enough tries the turbulent effect on the particle path will be statistically represented. For this project 10 tries were used.

5.3.1   Particle Size Distribution

The size of the particles generated from wood processing are rarely uniform but usaully follows a size distribution. One size distribution function that is often used and works well with solid waste particles such

as wood is the Rosin-Rammler distribution [36]. The Rosin-Rammler distribution is described by Equation 5.12.

$$Y_d = exp\left(-\left(\frac{d}{\bar{d}}\right)^n\right) \tag{5.12}$$

Here $\bar{d}$ is the mean diameter and n is a size distribution parameter that describe the spread of the diameters. This is used to describe Y_d which is the mass fraction of particles with a larger diameter then d. The density of the wood particles are set to 290 kg/m^3 [18]. The plotted Rosin-Rammler distribution function with three different spread parameter values can be seen in Figure 5.3.
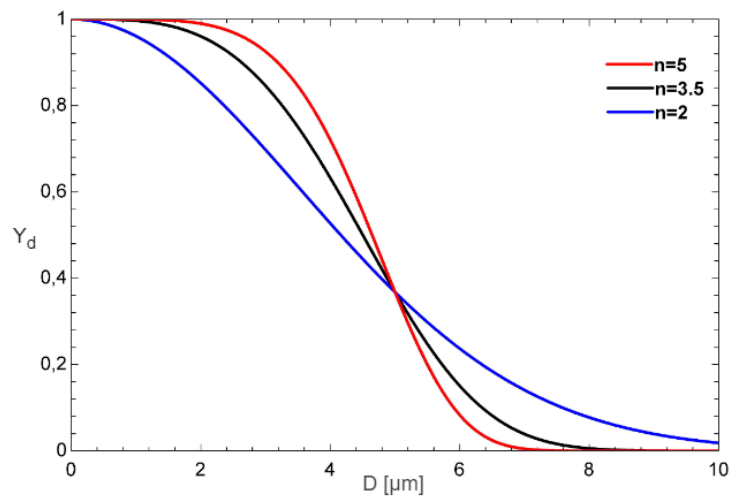
Figure 5.3: Rosin-Rammler diameter mass distribution. The mean diameter is set to 5 μm with a spread parameter of $n = 2, n = 3.5$ and $n = 5$.

For this project a spread parameter of $n = 3.5$ is used. The particle size distribution from Ansys Fluent with a spread parameter of $n = 3.5$ can be seen in Figure 5.4.
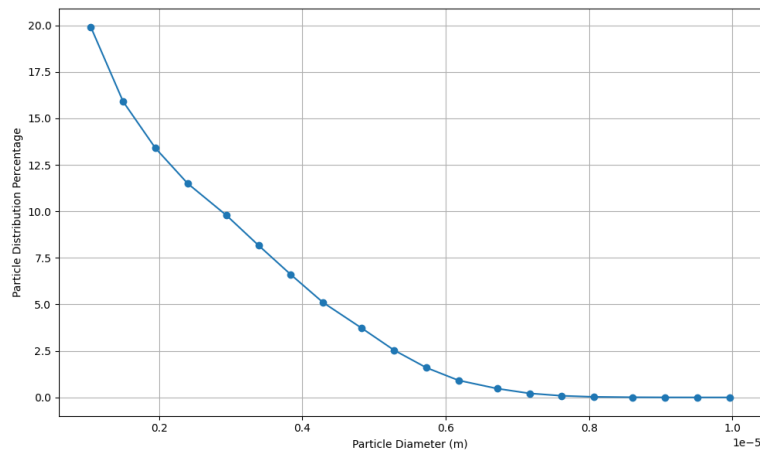
Figure 5.4: Particle size distribution in percent of the total particle injection.

It can here be seen that there are most of the small particles injected, though they make up a small percentage of the mass.

5.3.2 Particle Residence Time

In order to find the particle residence time, t_{res}, for a Stairmand cyclone separator, a number of particles where injected at a single timestep, and was monitored. The particle residence time for a single particle is defined as the time it takes a single particle to escape the cyclone. Therefore the trapped particles will not be considered for this. The number of particles escaped as a function of time can be seen in figure 5.5.
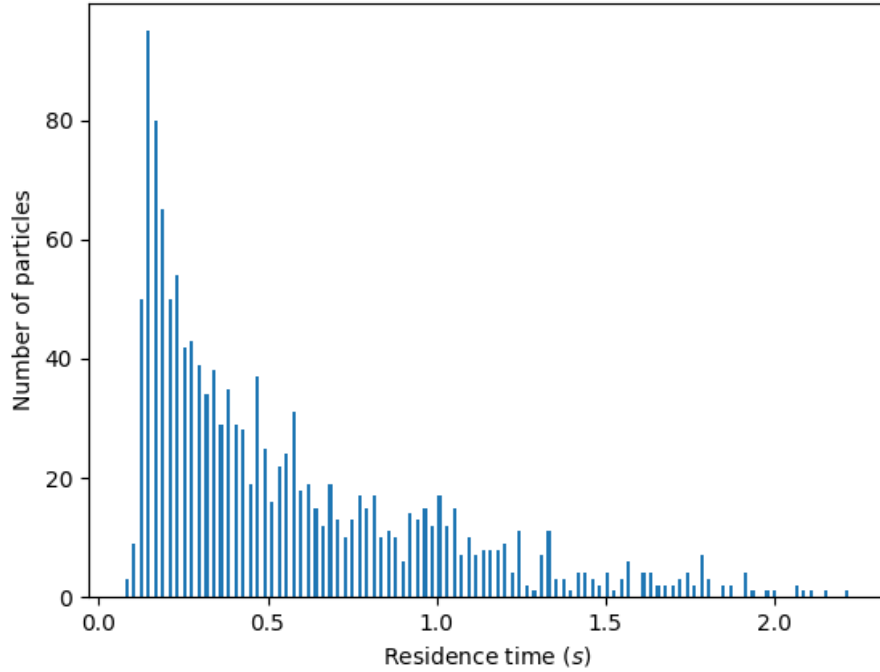
Figure 5.5: Residence time of escaped particles.

From Figure 5.5 it was found that the average residence time of the escaped particles was 0.56 seconds. It can be seen that some of the particle are in the cyclone for considerable longer then then others, with 90% of the particles leaving before 1.12 s and the median residence time of the particles being 0.41 s.

If this is compared to the gas residence time which is defined as the time it takes to replace all of the air in the cyclone separator $t_{gas} = V_{cyclone}/Q_{air}$. In this case the gas residence time was found to be 0.56 seconds, which is the same as the average particle residence time. The residence time in this project will therefore be taken as the average residence time of the escaped particles of $t_{res} = 0.56s$.

5.4 Solving Strategy

To obtain a fast converged solution the model is first simulated in steady state with a pseudo transient time step. The pseudo transient time step can help speed up convergence by introducing a local relaxation factor to the transport equation that are based on the Courant number in the cell instead of a constant under-realaxation factor [1]. The Courant number (CFL) is defined as:

$$CFL = \frac{v \cdot \Delta t}{\Delta x} \tag{5.13}$$

Where v is the fluid velocity, Δt is the timestep and x it the length of the cell. This is a measure of how many cells the flow is passing through in a timestep. For RANS simulations a CFL below 20-40 is recommended

[1]. For this simulation a Courant number of 5 was set to achieve convergence. This means that the pseudo timestep and thereby also the relaxation factor to the equations changes depending on the flow condition in each cell [1].

Furthermore the default under-relaxation factors of the variables are also applied.

$$\phi = \phi_{old} + \alpha\Delta\phi \tag{5.14}$$

This dampens the change in value between iterations by a constant factor α.

The steady state simulation is used to find a good starting guess for the transient simulation since the steady state simulation requires less computational time.

The simulation is thereafter switched to a transient simulation with relaxation on the higher order term included instead of the pseudo transient time step. This adds a relaxation factor of 0.75 to the terms higher then the first order term. This helps with stability and can also help prevent convergence stalling [1].

For the time discretization scheme a first-order implicit scheme was chosen. This makes it a stable unconditionally bounded scheme.

To choose an appropriate time step the Courant number is again considered so that it does not exceed 20-40. The simulation is then run until convergence.
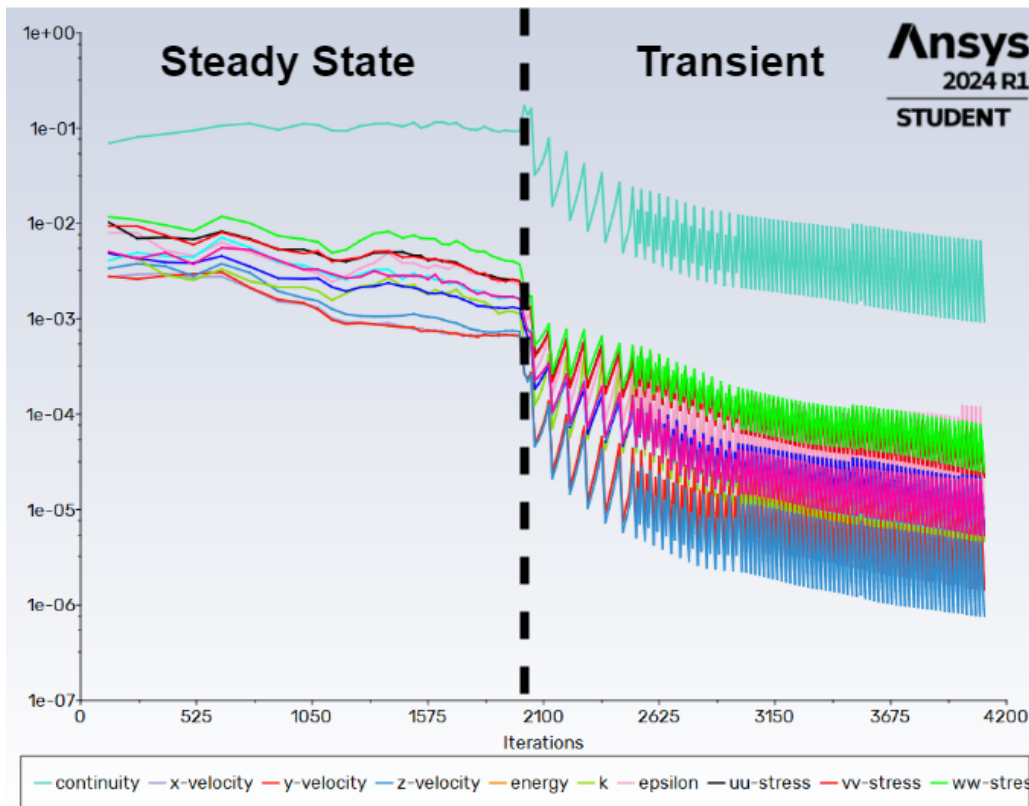

Figure 5.6: Residuals in steady state vs transient of the continuity, velocities and Reynolds stresses. Simulated for 2000 iterations in steady state and 0.55 s in transient, corresponding to approximately one residence time.

It can be seen on Figure 5.6 that the first part the simulation is run in steady state and then switched to transient with a timestep of 0.004 seconds and a convergence criteria of 10^{-3} with a maximum of 20 iterations per timestep. The residuals can be seen to drop approximately 2-3 orders of magnitude in the transient simulation. The change to transient simulation also have an impact on the pressure loss. Using only steady state the pressure loss was oscillating around an average value of 879Pa while the converged transient simulation settled at a single continuous value of 855Pa. The flow inside the cyclone is also considered to be transient by nature, with the inner vortex possibly becoming unstable for certain conditions [14]. Simulating in transient can also provide a better understanding of the particle trajectory. It was therefore concluded that it was necessary to include the transient simulation.

The residuals here are scaled so that the sum of the imbalances in the cells are scaled with respect to the sum of the cell values. This is in most cases more telling then the absolute residuals. It can be seen that the continuity residuals are a couple of magnitudes larger then the rest. This is because the continuity residuals are scaled with respect to the residuals at iteration number 5. This means that the scaled continuity residuals level are dependent on the residuals starting point.

5.5 Mesh

The mesh is constructed with polyhedral cells in the boundary layers and hexahedral cells in the core. The boundary layers are constructed with a constant first cell height and a constant growth ratio of 1.12. The boundary layers are extended out to the include most of the swirling flow in the cyclone which can be seen in Figure 5.7b. This is done to align the cells in the direction of the main flow to avoid false diffusion. At the bottom of the cyclone, where swirl is assumed to be the highest and the particles should separate from the air, a refinement zone is placed. This can be seen on Figure 5.8.
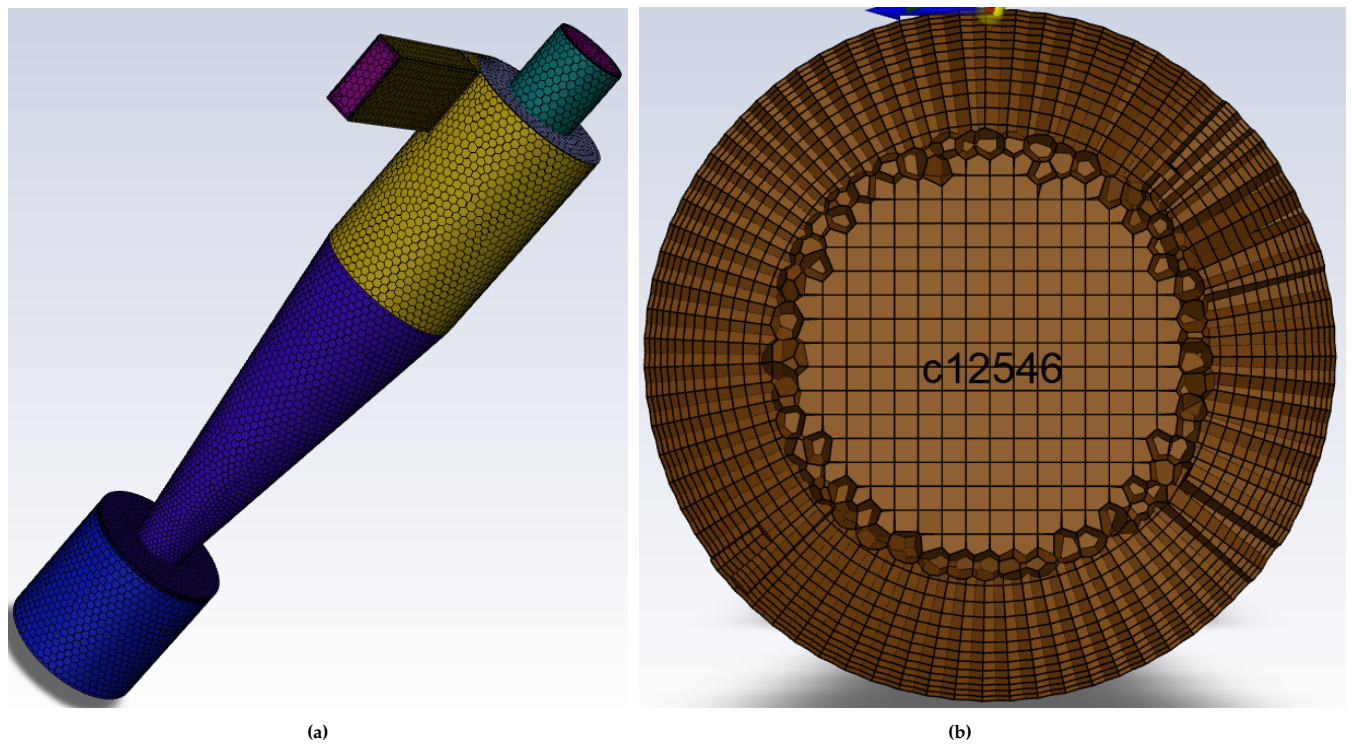
<div align="center">(a)</div>

<div align="center">(b)</div>

Figure 5.7: Polyhedral surface mesh of the cyclone 5.7a and cross section of cylindrical cyclone body with hex core 5.7b.

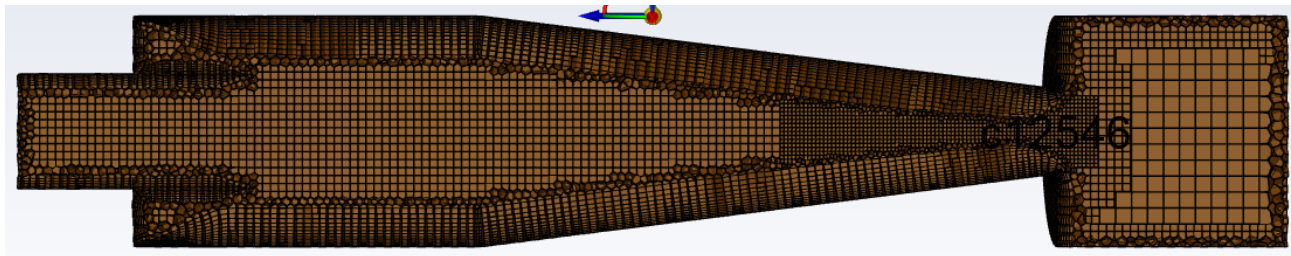<div align="center">

Figure 5.8: Cross section of cyclone.

</div>

The mesh is built up of a total of 177.000 control volume cells. The average skewness is 0.04 with a maximum of 0.8, which is a average well below the maximum recommended by Versteeg and Malalasekera [35], which states that the average should be below 0.35 and maximum of 0.8. The aspect ratio should be below 5 for the core mesh while the boundary layers can be up to 50 [35]. The mesh satisfy both of these criteria.
In order to verify if this mesh is sufficiently accurate a grid dependence study will be performed.

5.6   Grid Convergence Index (GCI)

For the GCI, two additional meshed were constructed in similar manner with a cell count ratio between the meshes of at least 2.2. One refined mesh with 442000 cells and one coarsened mesh of 74000 cells. The three

meshed all have the same first cell height from the walls but the growth rate and number of surface layers were varied between the three meshes to obtain overall similarity of the three meshes. All three meshes are also within the limits for skewness and aspect ratios. A cross section of the three meshes can be seen on Figure 5.9
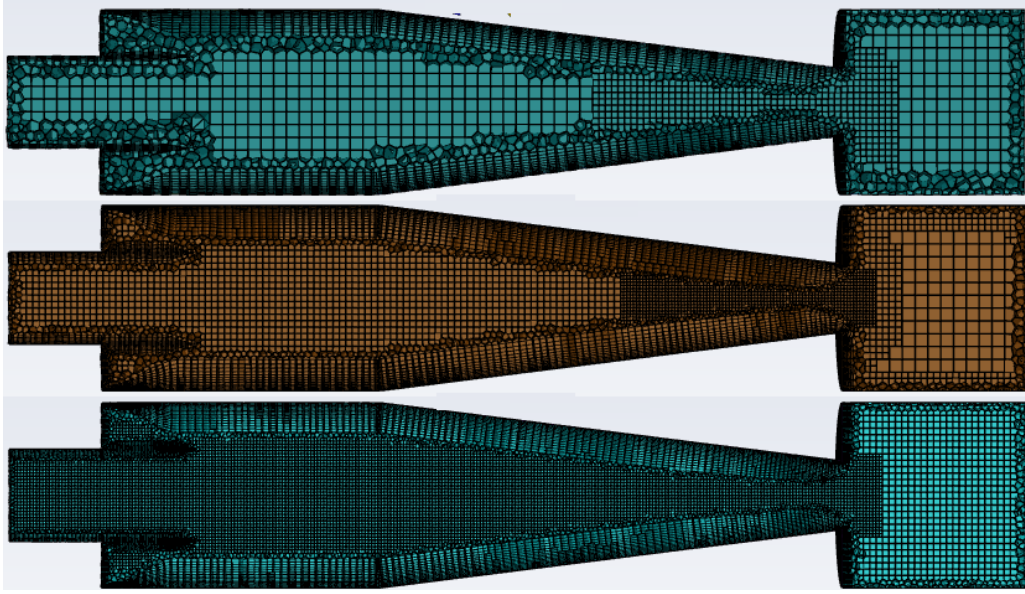

Figure 5.9: The three meshes used in the GCI.

The GCI will be calculated based on the approach presented by Celik et al. [4]. The value of interest ϕ, that are compared for the three meshes, will be the pressure loss across the cyclone.
By using the cell count refinement ratio N_2/N_1 and the difference in pressure loss $\Delta\phi$, the apparent order of which the simulation results approach the extrapolated exact solution can be found.

$$p = \frac{1}{\ln \sqrt[3]{\frac{N_f}{N_m}}} \left| \ln \left| \frac{\Delta\phi_{cm}}{\Delta\phi_{mf}} \right| + q(p) \right| \tag{5.15}$$

Here the subscript cm and mf refer to the coarse-medium and medium-fine. $q(p)$ is found in equation 5.16 and have to be solved iteratively with equation 5.15.

$$q(p) = \ln \left(\frac{\sqrt[3]{\frac{N_f}{N_m}}^p - s}{\sqrt[3]{\frac{N_m}{N_c}}^p - s} \right) \tag{5.16}$$

$$s = 1 \cdot \text{sign} \left(\frac{\Delta\phi_{cm}}{\Delta\phi_{mf}} \right) \tag{5.17}$$

The extrapolated exact solution can now be found in Equation 5.18.

$$\phi_{mf}^{ext} = \frac{\sqrt[3]{\frac{N_f}{N_m}}^p \cdot \phi_{fine}}{\sqrt[3]{\frac{N_m}{N_c}}^p - 1} \tag{5.18}$$

The approximate e_{mf}^a relative error can then be calculated as shown in equation 5.19.

$$e^a_{mf} = \left| \frac{\phi_{fine} - \phi_{medium}}{\phi_{fine}} \right| \tag{5.19}$$

The approximate relative error is then together with a safety factor F_s used to find the GCI_{fine} value showed in Equation 5.20.

$$GCI_{fine} = \frac{F_s \cdot e^a_{mf}}{\sqrt[3]{\frac{N_m}{N_c}}^p - 1} \tag{5.20}$$

The GCI_{fine} value estimates the solution error based on the fine grid. This can be seen as the error bars in Figure 5.10.
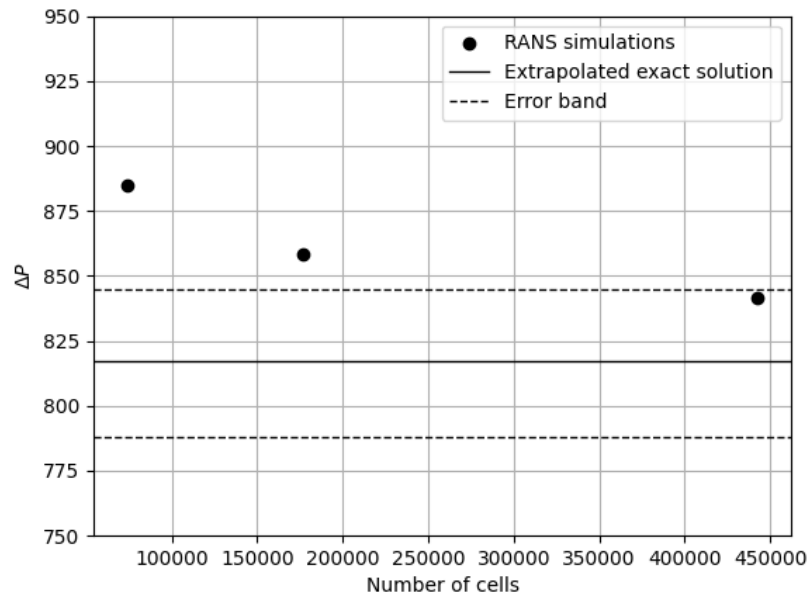
The results of the GCI can be seen in Figure 5.10 and Table 5.1.

Figure 5.10: Results of the GCI with each mesh and the extrapolated exact value.

It can be seen that the pressure loss generated by the fine mesh can be considered grid independent since it is within the error band set by the extrapolated exact value.

Parameter	Coarse	Medium	Fine	Exact
N	$74.14 \cdot 10^3$	$176.82 \cdot 10^3$	$442.23 \cdot 10^3$	-
ϕ	884.67	858.06	841.3	817.4
p				1.7
GCI_{fine}				3.5%

Table 5.1: The results of the GCI and the apparent order p.

The specific results for each mesh, as well as the exact extrapolated value and the approximate order, p, can be seen in table 5.1.

5.7 Validation

A comparison was also made of the tangential and axial velocity profiles of the cyclone, for each of the three meshes. The velocity profiles were measured in the cyclone $0.25D$ from the vortex finder as illustrated by the dotted line in Figure 5.11.
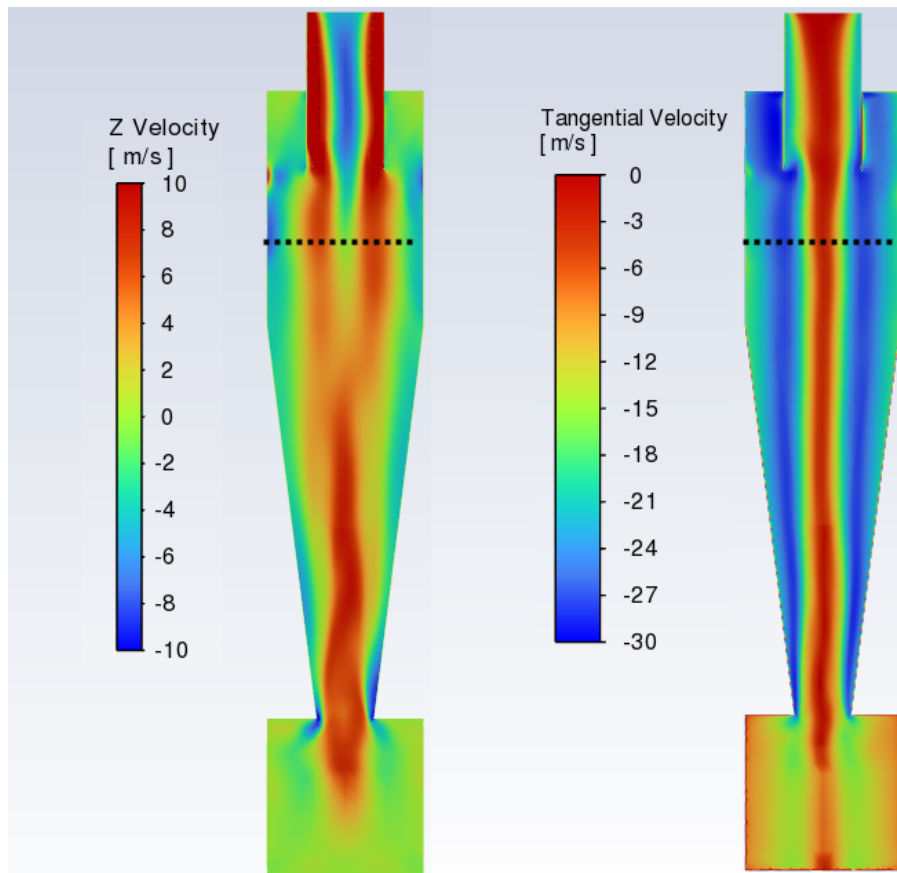
Figure 5.11: The axial and tangential velocity of the cyclone cross section simulated on the medium mesh, with measuring plane at the dotted line.

It can be seen from the simulation that there are some backflow from the outlet extending approximately down to the measuring plane. This is also verified by the experimental results obtained by Hoekstra [14]. This is the same experimental data used for comparison in Section 5.1.5.

The results of the three meshes and the experimental results can be seen in figure 5.12 and 5.13. In the figures the velocities are normalized with respect to the inlet velocity.
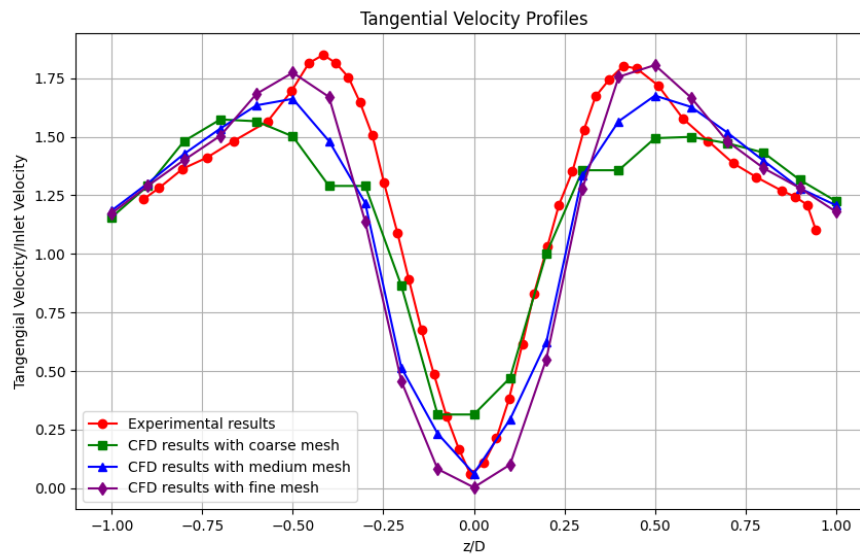

Figure 5.12: Tangential velocity profiles generated using the three different meshes, and compared to the experimental values.

Figure 5.12 shows that the coarse mesh and medium mesh underestimates the maximum swirl velocities, while the the fine mesh underestimates the swirl velocities in the core vortex.
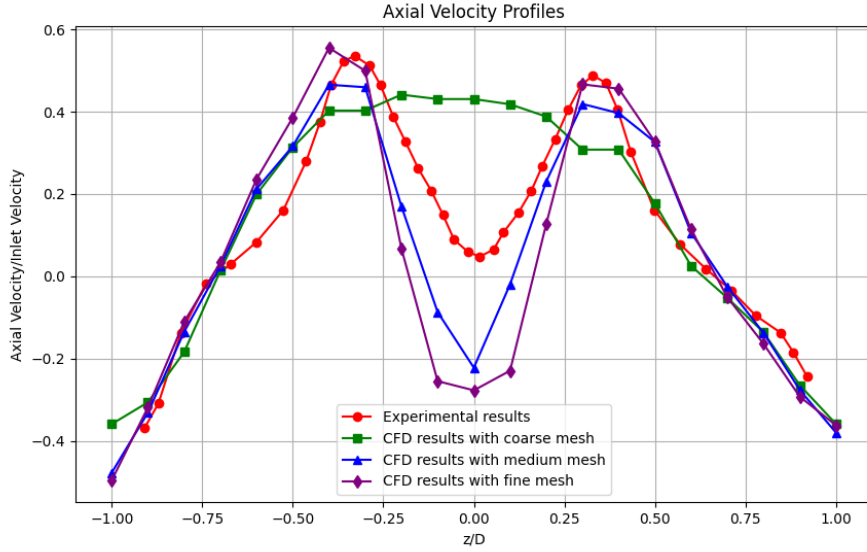
Figure 5.13: Axial velocity profiles generated using the three different meshes, and compared to the experimental values.

The axial velocity of the coarse mesh can be seen to completely miss the backflow, while the medium and fine mesh overestimates it a bit.

The medium mesh generates the best velocity profiles, while still generating a pressure loss that is fairly close to that of the fine mesh. Because of this, and the considerably faster simulation time, the medium mesh is chosen to be used for all simulations used in this project.

5.7.1 Particle Separation

To simulate the particle separation efficiency the Rosin-Rammler particle size distribution were used with a minimum and maximum diameter of 1 and 10 μm. The solid loading was set to 0.27 g/m^3 which corresponds to a volume loading of 10^{-6} so that one-way coupling and no particle-particle interaction can be assumed. This was chosen due to the extensive simulation time with a two-way coupling and particle-particle interaction model. In total approximately 25000 particles were tracked. This number is determined by the stochastic number of tries, the number of tracked diameters and the surface mesh.

Figure 5.14 shows the particle separation efficiency results for the CFD simulation plotted together with mathematical model. The correction factor, x_{fact}, and slope factor, m, are here adjusted to fit the simulation results with a correction factor of 0.8 and slope factor of 6, which is within reasonable correction values.
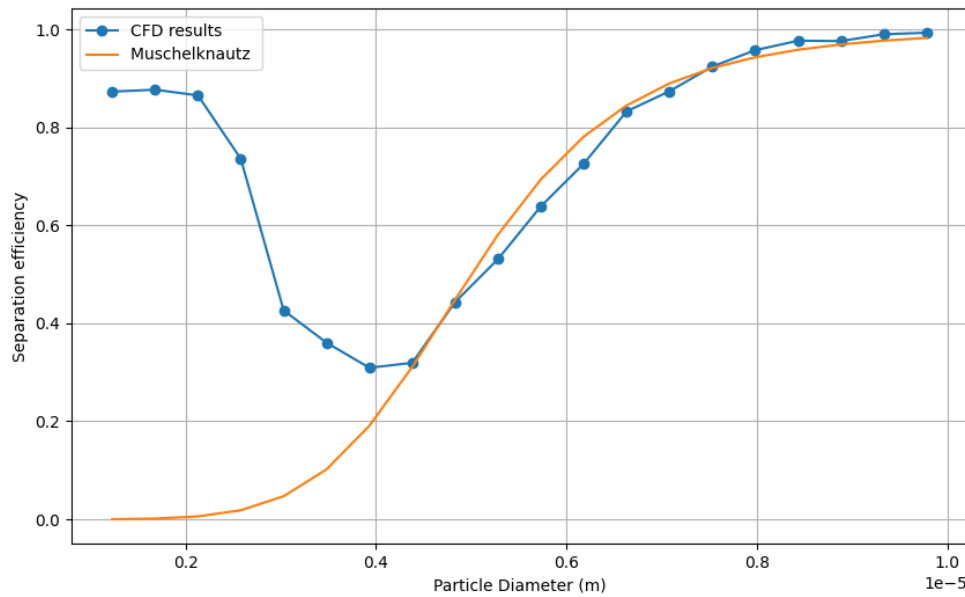
Figure 5.14: Simulated separation efficiency with a particle loading of $0.27 g/m^3$, compared to the separation efficiency calculated using the Muschelknautz method presented in section 4.3.

It can be seen in figure 5.14 that there is a higher separation efficiency at the lowers particle sizes, then when compared to particles with 3-5 μm. This is an effect not predicted by the mathematical model.

One would expect the separation efficiency to decrease towards zero or a constant value, as it is shown with the mathematical results. This is what is commonly expected with a decreasing particle diameter, it is, however, not the case for this simulation.

This is a common phenomena that can occur in cyclones dealing with small particle diameters. This is commonly referred to as the "fishhook" effect. It is not certain without doubt why this effect is occurring [15], but Hoffmann and Stein [15] believed that is likely caused by agglomeration, where the smaller particles collides with the larger particles and "stick" with them. The smaller particles could get stuck in the wake behind of larger particles due to the pressure gradient. Agglomeration could also occur due to a electric charge of the particles or due to humidity [15].

Other researchers attributed the fishhook effect to particle agglomeration caused by Van der Walls attractive forces between the particles. These forces increases as the particle size decreases, causing the particles to agglomerate and therefore behave like larger particles [38].

Another explanation for the fishhook is that it is because of the flow conditions. A study was made by Roldán-Villasana, Williams, and Dyakowski [27] who argued that the fishhook effect is attributed to eddies in the system.

According to Majumder, Yerriswamy, and Barnwal [20] the fish-hook effect is a natural behavior of ultra fine particles, in a centrifugal force field. It is caused by the sudden drop in settling velocities in the transition from

the Stokes flow regime to the transitional flow regime. As shown in the following equations, the equation for the terminal settling velocity, v, is dependent on whether the particle is within the Stokes flow region. Here the Stokes regime is taken as $Re_p<0.2$.

$$v = \frac{(\rho_p - \rho_f)D_p^2\omega^2 r}{18\mu} \qquad\qquad 10^{-4} < Re_p < 0.2$$

$$v = \left(\frac{\omega^2 \cdot r}{g}\right)^{1/2} v_g \qquad\qquad 0.2 < Re_p < 500$$

With ω being the angular velocity and v_g being the settling velocity of a particle in a gravitational force field.[20]

Since the fishhook is present in the CFD simulation with one-way coupling and no particle-particle interaction the reason for the fishhook cannot be attributed only to agglomeration since this is not modeled. This indicate that the flow conditions or the possibly the Stokes number or settling velocity could be the reason for the fishhook.

Experimental data from Hoffmann and Stein [15] showed that the fishhook is affected by the solid loading ratio as seen in Figure 5.15.
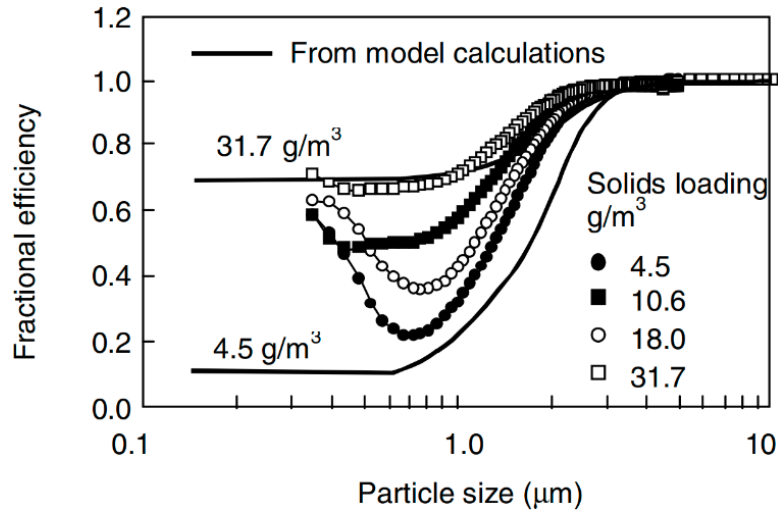

Figure 5.15: Figure from Hoffmann and Stein [15] showing experimental separation efficiency at different solid loadings. The model calculation is from the Muschelknautz model.

The experimental results shows that the fishhook does occur and with higher solid loading, the effect become more damped with the cyclone having a higher overall efficiency. It can also be seen that the Muschelknautz model does predict the separation efficiency well at high solid loadings, but fails to predict the fishhook effect on lower solid loadings.

One possible explanation for the solid loading affecting the separation is the critical mass loading. This is the maximum amount of mass that the turbulence in the gas phase can support against gravity.

If the mass loading is higher than the critical mass loading, the excess mass loading higher then the critical mass loading will be centrifuged to the cyclone wall and separated out while the critical mass load will stay in turbulence suspension and separated out according to the otherwise separation efficiency. [15].

This increased efficiency at higher solid loading could also both be due to particles collisions or the particles affecting the flow. It was therefore investigated whether interaction between the two phases could show an effect on the fishhook by increasing the solid loading from 0.27 g/m^3 to 27 g/m^3. The result of this can be seen in Figure 5.16.
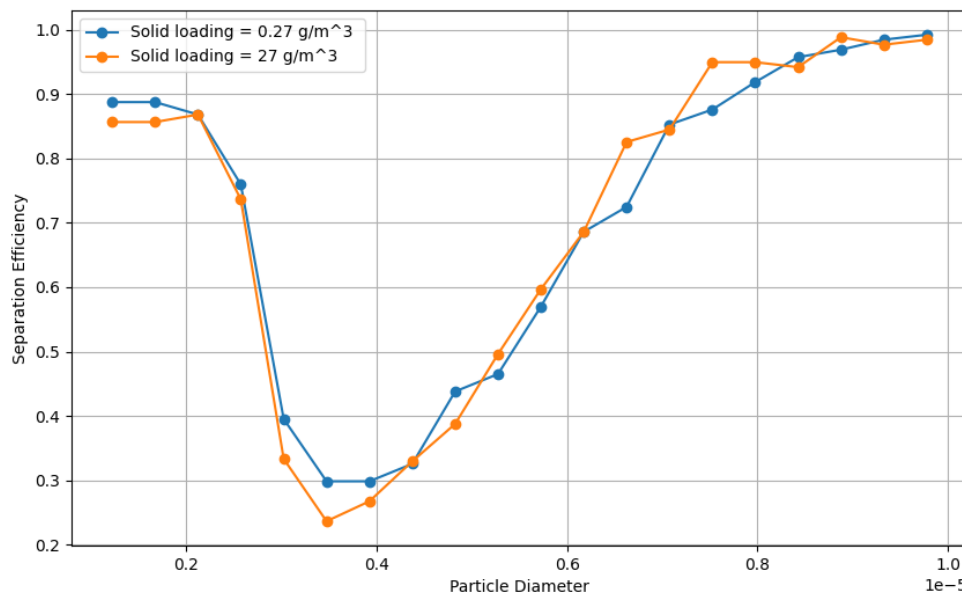

Figure 5.16: CFD simulation of separation efficiency at two different mass loadings.

It can be seen that the results are practically identical, which shows that the particle-particle interaction modeling is necessary to show the effect off a higher solid loading. It has however not been possible to successfully model particle collisions due to excessive simulation time and convergence issues.

Since it is not certain without doubt how or why the fishhook effect is occurring it will therefore be investigated further what influences this effect.

6 Investigation of the Fishhook Effect

In this chapter the fishhook effect and backflow will be investigated further to find how different parameters influence these phenomena. It will be investigated whether the fishhook effect is dependent on geometrical parameters or the flow conditions.

6.1 Investigation of Particle Movement

In this section the behavior of the particles in the cyclone separator is investigated in order to gain a better understanding of the particle movements and how this affects the escaped and trapped particles. In Figure 6.1 a cross section of the 2D velocity vector field of the cyclone can be seen.
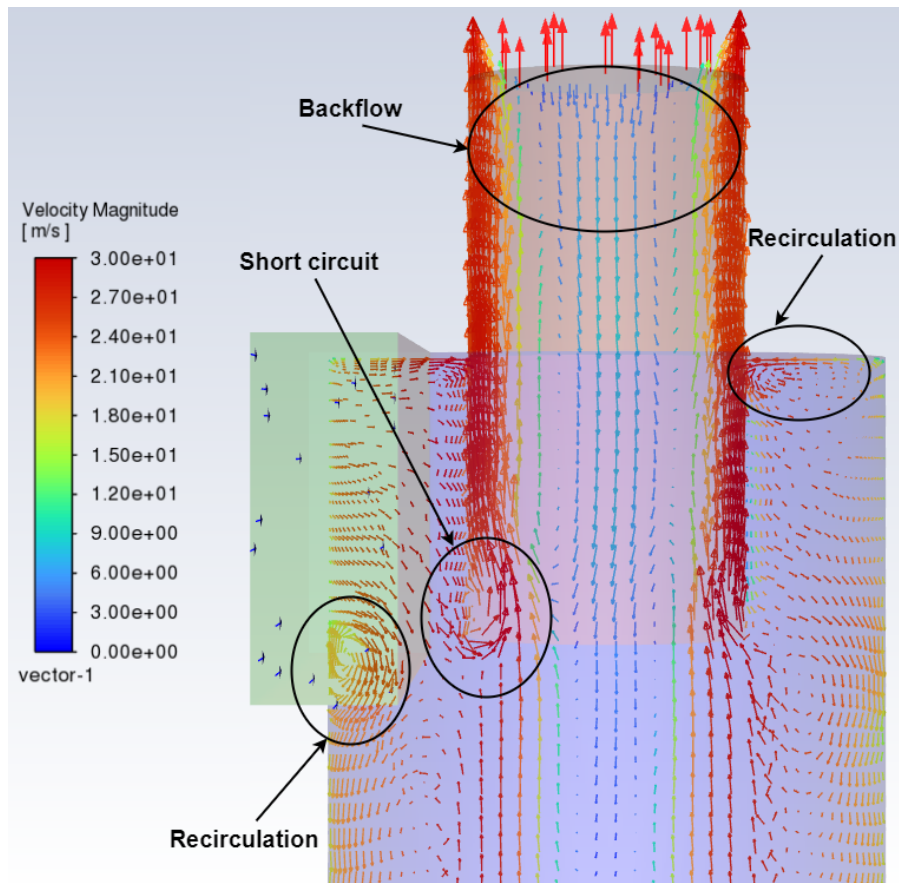

Figure 6.1: Projected velocity magnitude vector field of the cross section through the middle of the cyclone.

Figure 6.1 shows some recirculation areas at the top of the cyclone and underneath the inlet duct. The backflow can also be seen extending from the outlet and down into the cyclone. At the end of the vortex

finder an area with short circuit can be seen. Some particles will enter the vortex finder and escape without reaching the bottom of the cyclone.

To investigate which particle sizes are escaping through the short circuit, a particle injection will be simulated entering a cyclone without particles. The injection will be over 0.1 residence time and the particles that escape through the outlet will then be sampled for 0.6 residence time. This means that the particles that escape through the outlet in this time interval will have short circuit and not made it to the bottom of the cyclone. In Figure 6.2 the particle development through time and space can be seen for different diameters. The same particle distribution as showed in section 5.3.1 is used.
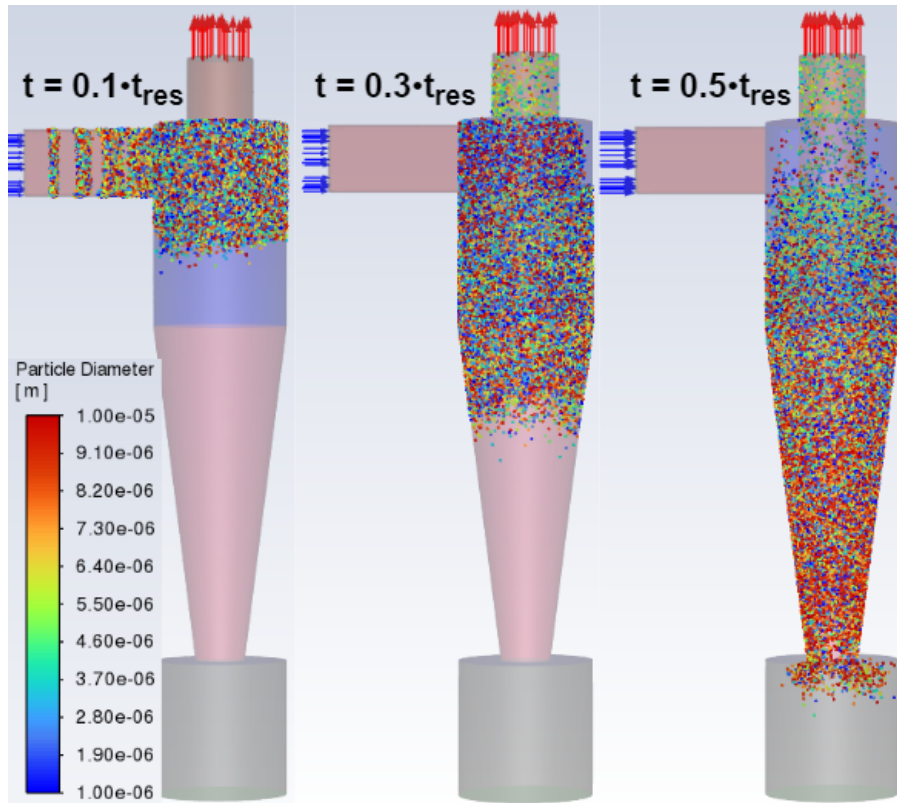

Figure 6.2: Particle movement through time and space using unsteady particle tracking at 0.1, 0.3 and 0.5 residence time.

The results of the simulation can be seen in Figure 6.3, showing the fraction of the different particle diameters escaping through the outlet due to short circuiting.
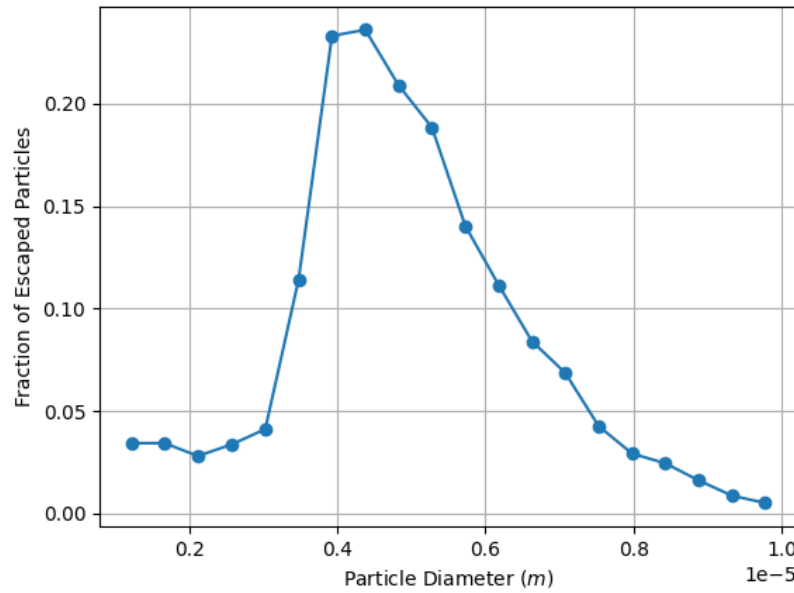
Figure 6.3: Fraction of particles that escape through the outlet due to short circuiting.

In this simulation 8.5 % of the particles escaped which is approximately a third of the particles when compared to the overall efficiency.

It can be seen that the majority of the particles that short circuit and escape are in the range of 3.5-6 μm. This is the same range that the cyclone has a low separation efficiency.

This shows that the flow in the cyclone affect different particle sizes differently and it is not necessarily the smallest particles that follow the flow most closely that escape through the short circuit, as one might think. This fishhook effect could change with changing flow conditions inside the cyclone or could also be different in a geometrical different cyclone.

6.2   Obermair and Staudinger Cyclone

To investigate if a change in geometry could change affect the fishhook effect, a different kind of cyclone was simulated. The cyclone simulated was an Obermair and Staudinger cyclone documented in Hoffmann and Stein [15]. This cyclone can be seen in Figure 6.4 with geometrical measurements. The main difference from the Stairmand cyclone is that the Obermair and Staudinger cyclone is shorter, with the cone under being half the length, than that of the Stairmand Cyclone.
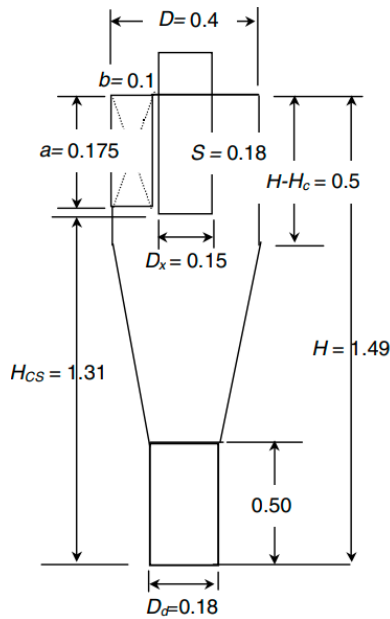
Figure 6.4: The Obermair and Staudinger cyclone with measurements in meters.

The mesh was constructed in a similar manner. The inlet velocity was set to 22.5 m/s, which has equal Stokes number and under the assumption of geometrically similarity should have the same cut size as the Stairmand cyclone. The cyclones are not geometrically similar but should give a cut size fairly close to the Stairmand cyclone. The results of the separation efficiency can be seen in Figure 6.5.
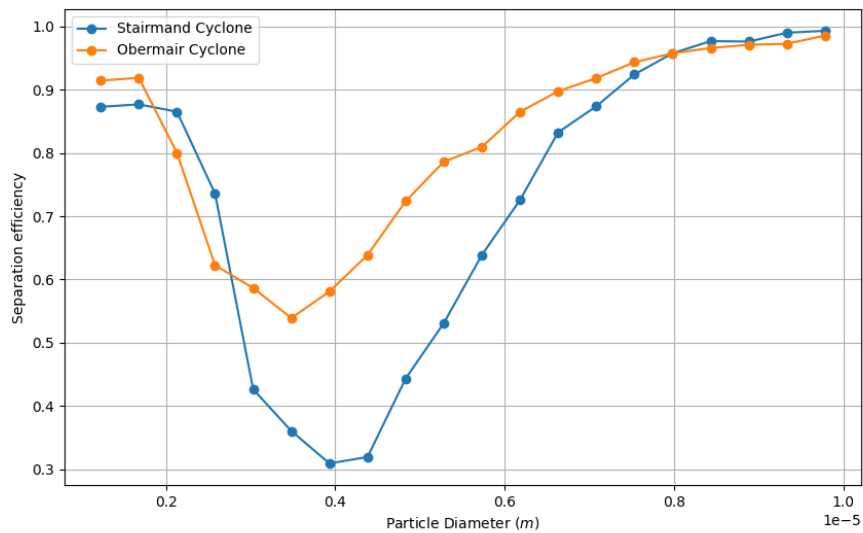

Figure 6.5: A comparison of the simulated separation efficiency of a Obermair cyclone and a Stairmand cyclone at equal stokes number.

It can be seen that the fishhook effect is still occurring in the approximately same location as the Stairmand

cyclone but with a higher overall efficiency. A change in geometry did not have significant change to the fishhook effect when the Stokes number was equal.

To test if a change in flow conditions inside the cyclone have an effect on the fishhook the inlet velocity will be varied. This changes both the Stokes number and Reynolds number and could therefore also change the fishhook.

6.3   Varying Inlet Velocity

According to the mathematical methods presented in section 4.2, the particle cut size should decrease when the inlet velocity is increased. It is, however, not known how the inlet velocity will affect the fishhook. The results at different inlet velocities can be seen in figure 6.6.
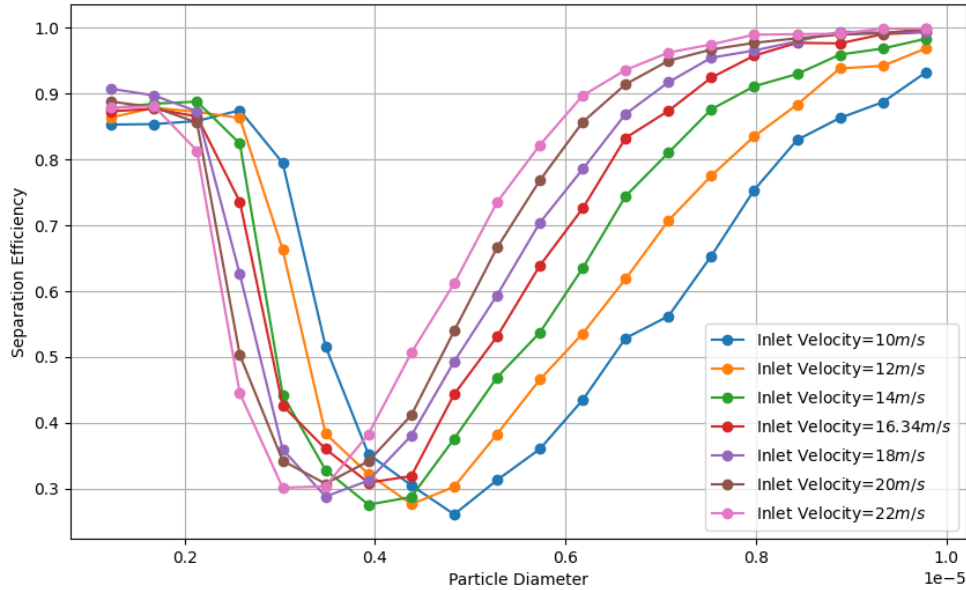

Figure 6.6: A comparison of the separation efficiency at various inlet velocities.

It can be seen that the cut size increases as the inlet velocity is decreased, as expected.

The fishhook can be seen to shift with the cut size towards larger diameters at lower velocities, while increasing the range of high separation efficiency at the smallest particles. This indicate that the window of low separation efficiency is dependent on either the Reynolds number or Stokes number.

The pressure loss results from the CFD simulation with varying inlet velocity was also compared to the mathematical model and experimental data in Figure 6.7.
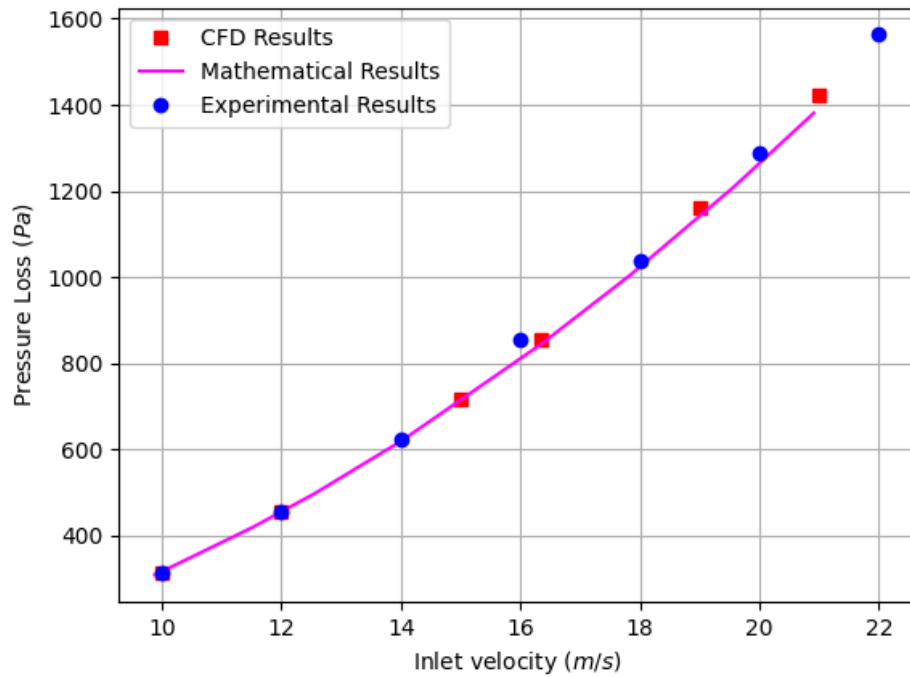
Figure 6.7: Pressure loss as a function of inlet velocity for both the CFD, experimental results and the mathematical model.

It can be seen that there is an increase in pressure loss as the inlet velocity is increased, which follows the general trend by the mathematical model and experimental data. The general increase in pressure loss, is of course not favorable, but with the increase in overall separation efficiency a optimum would have to be found matching the system in which the cyclone will operate.

The impact on the backflow can be seen in Figure 6.8. The backflow was normalized with respect to the inlet velocity, as shown in equation 6.1, and measured across the middle of the vortex finder.

$$\text{Normalized Velocity} = \frac{\text{Axial velocity across vortex finder}}{\text{Inlet velocity}} \tag{6.1}$$
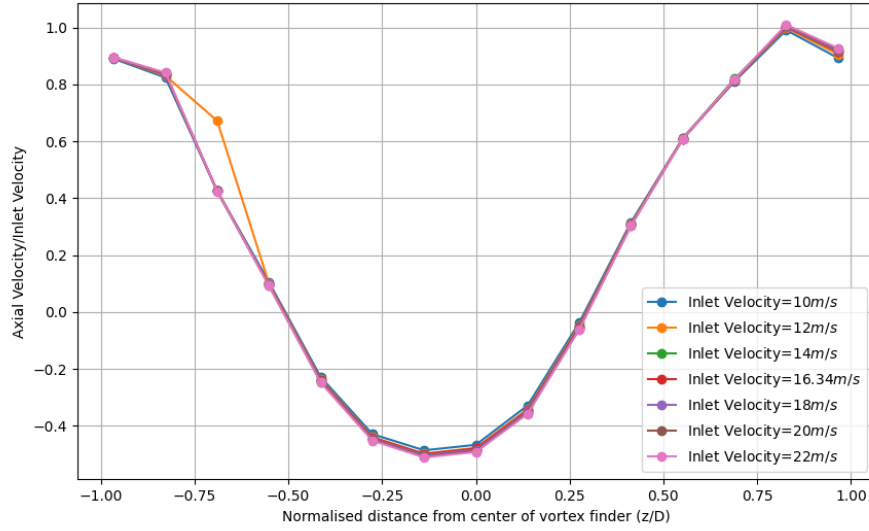
Figure 6.8: Normalised velocities with respect to inlet velocity in the vortex finder.

From the normalized velocity profile it can be seen that the backflow is proportional to the inlet velocity. A decreased backflow could decrease the velocity at the vortex finder wall and thereby also increase the static pressure. A lower pressure difference between the vortex finder and the outer vortex could decrease the amount of air short circuiting.

There might be improvements to the pressure loss or separation efficiency if the vortex in the vortex finder is disturbed, in order to prevent backflow. This could be done using similar methods as those in section 2.3.2. As mentioned in the problem analyses a bend or outlet restriction could decrease the pressure loss or increase the separation efficiency. It will therefore be investigated how different bends affect the pressure loss, separation efficiency and backflow since it is not well investigated what effect the backflow has on these.

6.4　Investigation of Outlet Bend

In order to investigate whether or not the cyclone performance is affected by the outlet design, two different bends where designed and simulated on the outlets. Except for the outlet all other design and operation parameters were identical to that of the original cyclone. One of the outlets was a rounded bend placed directly atop of the vortex finder with a bend radius of $2D_x$ and the other was a sharp square bend with a distance to the top of the vortex finder equal to $1D_x$. This can be seen in Figure 6.9.
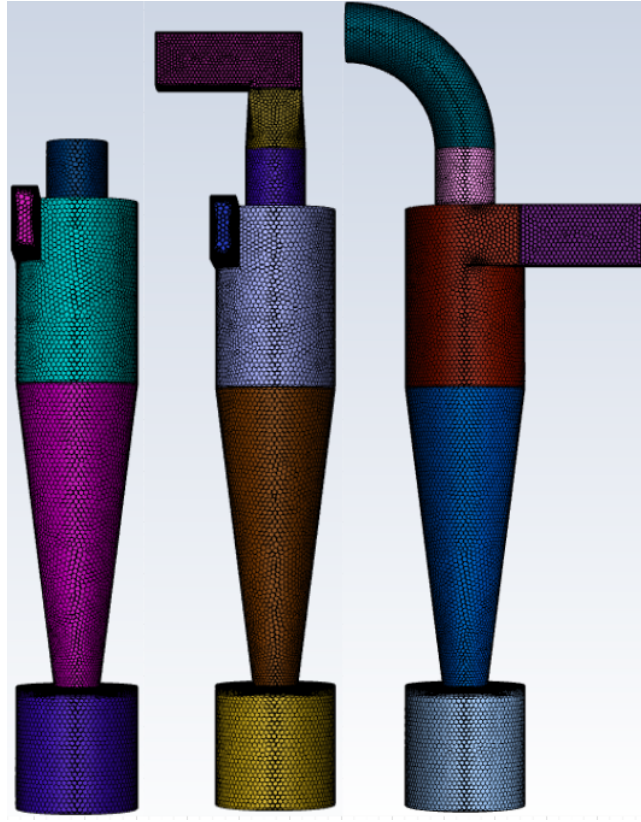
Figure 6.9: The two different outlet bends compared to straight outlet.

The results can be seen in table 6.1 as well as Figure 6.10 and 6.12.

Outlet type	Pressure loss [Pa]	Bend Euler number	η_s
Rounded bend	946	0.18	69.2
Sharp bend	1103	1.1	68.6
Straight (original)	855	-	67.6

Table 6.1: The overall separation efficiency, pressure loss and bend Euler number of the various outlet designs simulated. Euler number found from Idel'chik [16]

The bends can be seen to increase the pressure loss of the cyclone. If the bends are calculated as an additional pressure loss to the standard cyclone using the Euler number and the average axial outlet velocity of $7.2\,m/s$, it can be found that the pressure loss of the rounded bend is 5.6 Pa and 34 Pa for the sharp bend. The additional pressure loss for the bends can be seen to be significantly higher with 91 Pa and 248 Pa for the rounded and sharp bend respectively. This is because the Euler number is based on a fully developed turbulent flow profile, which is not the case here. It can be seen in Figure 6.10 that the axial velocity in the vortex finder has backflow in the center while reaching nearly 15 m/s at the vortex finder wall. In addition to this, the flow is also swirling, reaching velocities of up to 30 m/s.
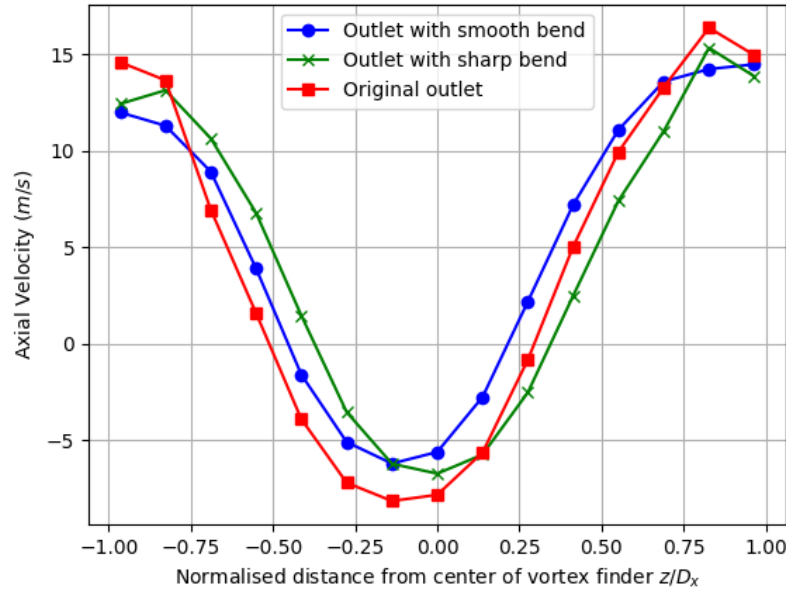
Figure 6.10: Comparison of the backflow velocities, for a regular outlet and the two bend outlets.

It can be seen that a bend on the outlet did not do a significant change in the backflow, but there is a small decrease in backflow compared to a straight pipe. This is the case for both a rounded and sharp bend.
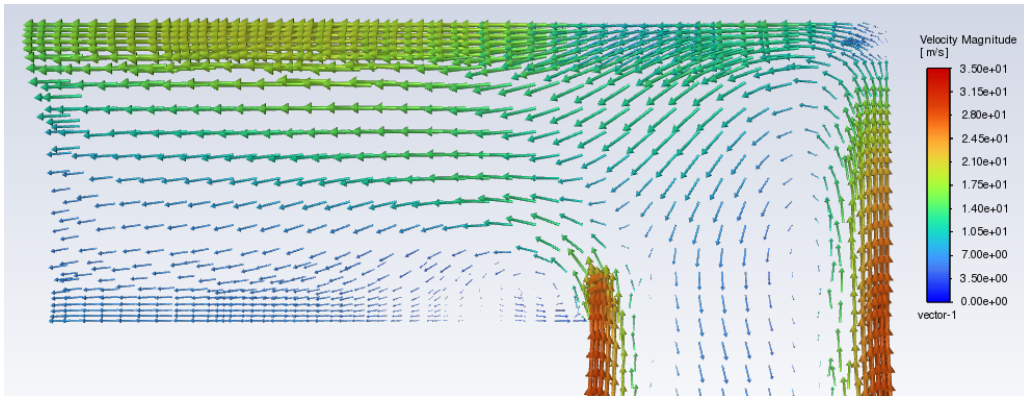

Figure 6.11: Projected velocity magnitude vector field of the sharp outlet bend.

It can be seen in Figure 6.11 how the backflow in the sharp bend does not extend all the way to the outlet but occurs by recirculating flow in the sharp bend and reentering the cyclone. This is expected to be part of the reason for the significant higher pressure loss in the bend.
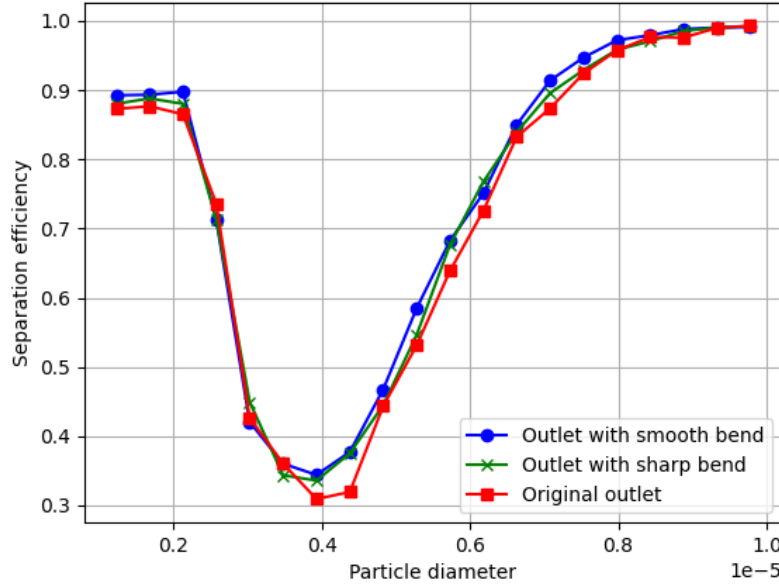
Figure 6.12: Comparison of the separation efficiency, for a regular outlet and a bend outlet.

It can also be seen on the separation efficiency that the outlet bends did not change the general behavior of the particles. Overall there was a small increase in efficiency but a significant increase in pressure loss.

In order to investigate whether the particle separation can be affected by the outlet conditions, the diameter of the vortex finder is varied, in order to investigate how this affects the backflow, pressure loss, short circuit and overall separation efficiency.

6.5   Investigation of Vortex Finder Diameter

An increase in the vortex finder diameter (D_x) should lead to a decrease in pressure loss, and vice versa [15]. In order to investigate how such a change would affect the separation efficiency and the backflow, three different cyclone designs have been made. These designs are identical to the original cyclone in design and input parameters, except for the diameter of the vortex finder which is changed to 0.3D, 0.4D and 0.6D for the new cyclone designs. The results can be seen in table 6.2 as well as figure 6.14 and 6.13.

Vortex Finder Diameter	Pressure Loss [Pa]	η_s
$D_x = 0.3D$	1613	74.3
$D_x = 0.4D$	1205	69.8
$D_x = 0.5D$ (original)	855	67.6
$D_x = 0.6D$	696	53.7

Table 6.2: A summary of the main simulation results found by changing the vortex finder diameter.

A decrease in vortex finder diameter (D_x) generally leads to a increase in pressure loss, but also leads to higher overall efficiencies.

The higher overall efficiencies of the cyclones with decreased vortex finder diameter is caused by the higher efficiency at smaller particle sizes, which take up a majority of the total number of particles in the particle distribution.
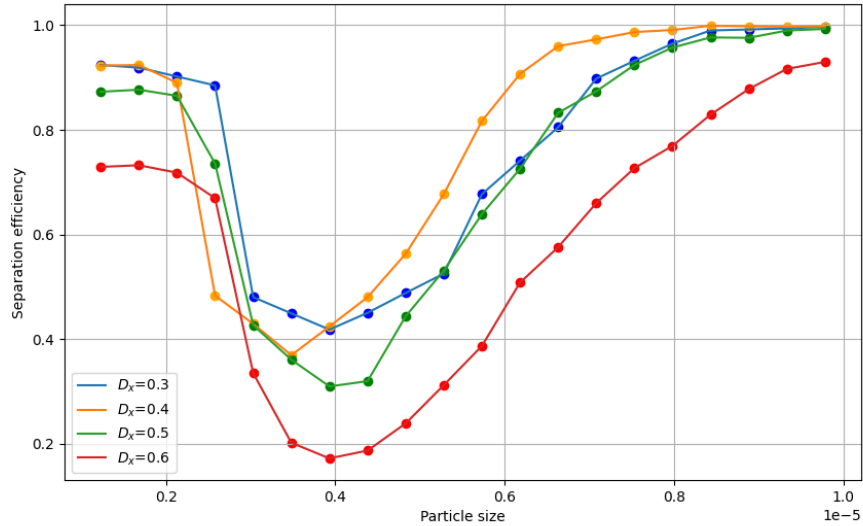

Figure 6.13: Separation efficiency with various vortex finder diameters, D_x.

It can be seen in figure 6.13 that a vortex finder diameter of 0.4D gives a better efficiency for the larger particles, and a decrease in cut size of almost one micrometer compared to $D = 0.5$. In Figure 6.14 the vortex finder velocity profiles for the four cyclones are compared.
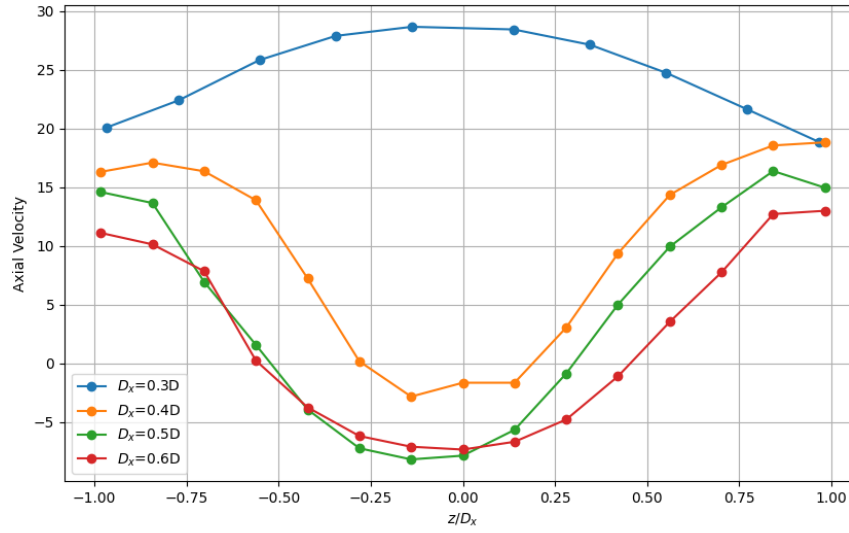
Figure 6.14: The velocity profiles in the vortex finder with different vortex finder diameters.

Here it can be seen that the backflow is in general decreasing with decreasing vortex finder diameter. There seems to be limit between the decrease in vortex finder diameter and back flow between $D_x = 0.3D$ and $D_x = 0.4D$, where the $D_x = 0.3D$ has no backflow but looks more as a developed pipe flow profile.

6.5.1 Vortex Finder Diameter Influence on Short Circuit Particles

In order to investigate if the improvement in separation efficiency with a decreased vortex finder diameter comes from a decrease in the number of particle that short circuit, a simulation was made similar to that in section 6.1. A comparison of the results for the short circuit fraction of the $D_x = 0.4D$ and $D_x = 0.5D$ can be seen in figure 6.15.
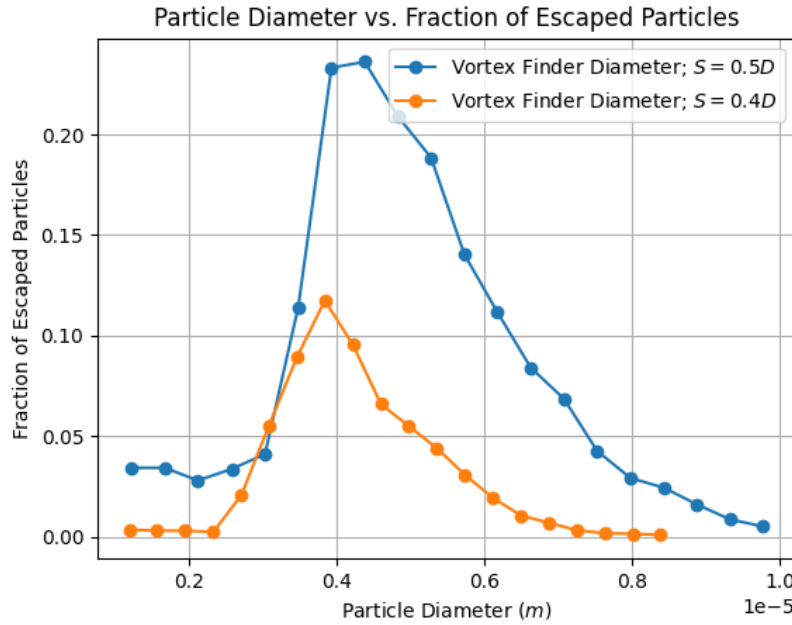
Figure 6.15: Comparison of the short circuit particles, for two Stairmand cyclones with D_x=0.5D and D_x=0.4D.

It can be seen that a considerably smaller fraction of particles escapes via short circuit, when the vortex finder diameter is reduced to 0.4D.

It was also investigated if the length of the vortex finder could have an affect in limiting the short circuiting as well as the backflow. This did however not show a significant effect on the backflow or the fishhook.

It is therefore still uncertain how or why the fishhook effect is occurring, but it was found that the fishhook placement with respect to the particle sizes could be shifted by changing the flow conditions inside the cyclone. The fishhook effect could possibly be taken advantage of by scaling cyclones so they capture different ranges of diameters.

6.6   Scaling of Cyclone

In this section, the effect of cyclone size, and the impact it has on separation efficiency and pressure loss will be tested out. In order to do this, the previous tested Stairmand cyclone will be scaled up and down in size. Two different scalings will be tested and compared in this section; a Stairmand cyclone with half the diameter, and a cyclone with double the diameter.

It was previously found that the inlet velocity could shift the placement of the fishhook effect. By changing the velocity both the cyclone Reynolds number and the Stokes number changes, so it is not clear which one contributes to the rise of efficiency for the small particles in the fishhook. By scaling the cyclone to different sizes and inlet velocities this can be tested using with the scaling laws.

A table of the simulated cyclones can be seen in table 6.3.

Cyclone Diameter (mm)	Inlet velocity m/s	Pressure Loss Pa	Eu	η_s
145	8.17	197	4.9	60.3
145	16.34	818	5.1	61
290 (Original)	16.34	855	5.3	67.6
580	8.17	218	5.4	74.2

Table 6.3: The overall separation efficiencies, pressure loss and Euler number of the scaled cyclone, with varying inlet velocities.

The higher efficiencies of the larger cyclones are once again the effect of the skewed particle distribution.

It can be seen from Table 6.3 that the scaling of the pressure loss overall approximately have a constant Euler number and scale with v^2. It can however also be seen that the trend that the Euler number for high Reynolds numbers should slightly decrease with increasing Reynolds number does not apply to the for the small cyclone here. This is because the Reynolds number of the small cyclone is sufficiently low, that the friction factor is no longer independent of the Reynolds number. This leads to an increase in the friction factor, which decreases the Euler number [15].

By using half the diameter but also half the inlet velocity the separation efficiency curves should look similar according to the scaling laws, since this results in the same Stokes number. This can be seen to be true in Figure 6.16 as the green and blue curve.

By doubling the cyclone diameter and halving the inlet velocity, the cyclone will have the same Reynolds number but only a quarter of the stokes number, for the same particle size.

This increases the cut size but it was uncertain where the fishhook would reach its lowest point. It can be seen from the red curve that the fishhook does shift to reach its lowest point at a higher particle diameter, which shows that it depends on the Stokes number. The same shift can be seen for yellow curve with half cyclone diameter and the same inlet velocity.
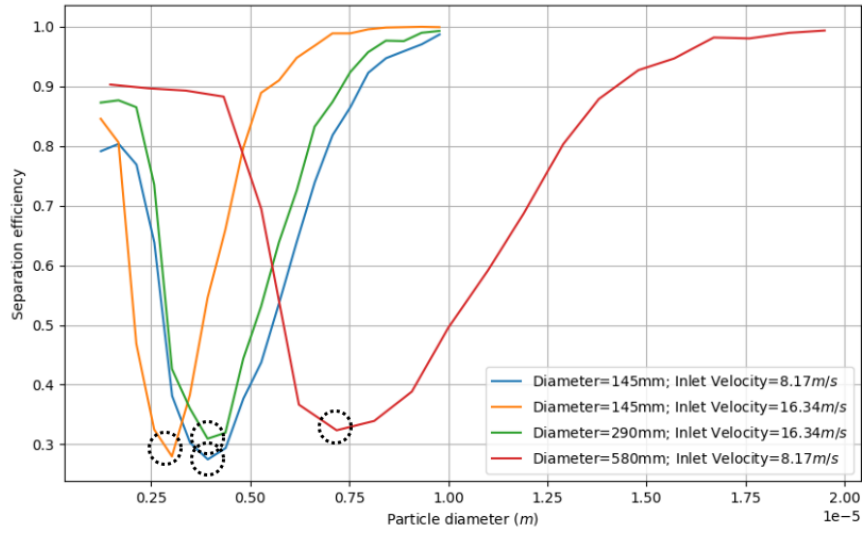
Figure 6.16: Comparison of separation efficiencies of scaled cyclones with different velocities. Dotted circles showing where the fish hook effect starts.

It can be seen that the fishhook beginning point shifts with the cut size. In Figure 6.16 the minimum efficiency point, which is where the fishhook effect begins is marked by a dotted circle. If the Stokes number of this point is plotted against particle size for various cyclone scaling and velocities, Figure 6.17 is obtained.

For reference the Stokes number for particles 1-10 μm in the Stairmand cyclone of 290 mm with inlet velocity of 16.34 m/s is also plotted.
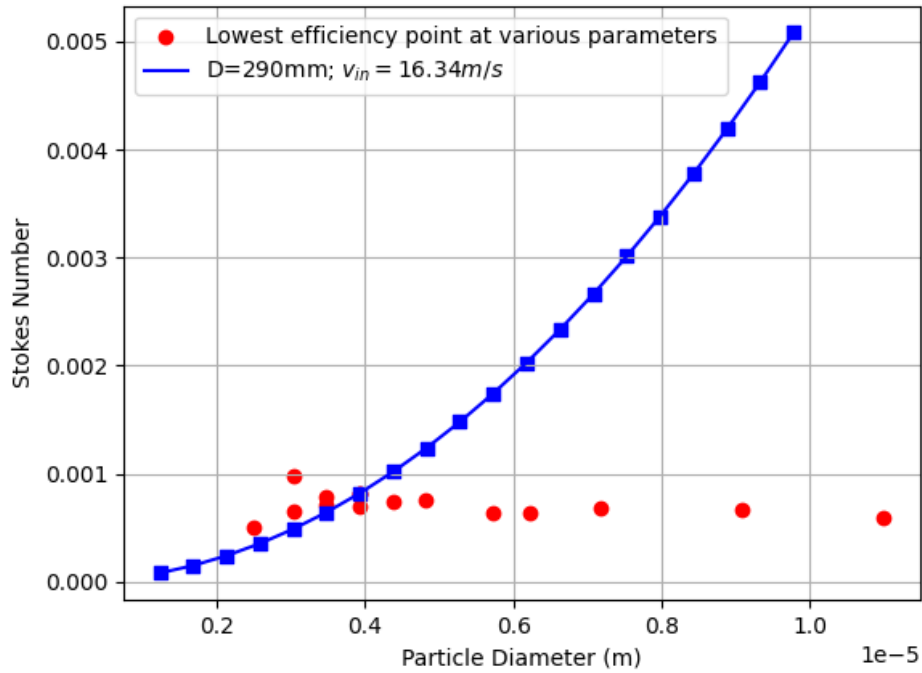
Figure 6.17: Stokes numbers for particles where the fishhook starts for Stairmand cyclones with various inlet velocity and cyclone diameter. The blue line is Stokes numbers for cyclone D=290 mm for scale.

It can here be seen that the Stokes number for where the fishhook starts in the Stairmand cyclone is approximately constant across scaling and inlet velocities, with an average Stokes number of $7 \cdot 10^{-4}$.

This emphasises that the occurrence of a fishhook beginning point is at a specific stokes number.

This means that the scaling laws for a geometrically similar cyclone also apply to where the fishhook effect starts. This Stokes number could change in a geometrically different cyclone. If this is compared to the Obermair cyclone simulated in Section 6.2, the fishhook starts at $6.4 \cdot 10^{-4}$, which is approximately the same, but for a geometrically different cyclone.

To investigate whether this occurrence of the fishhook ,at an approximate constant stokes number, is related to the particle Reynolds number and settling velocities, as mentioned by Majumder, Yerriswamy, and Barnwal [20], the particle Reynolds number throughout the cyclone was tracked at 3 different particle sizes. This was done by inputting an uniform particle size of 1,4 and 7 μm as seen on Figure 6.18.
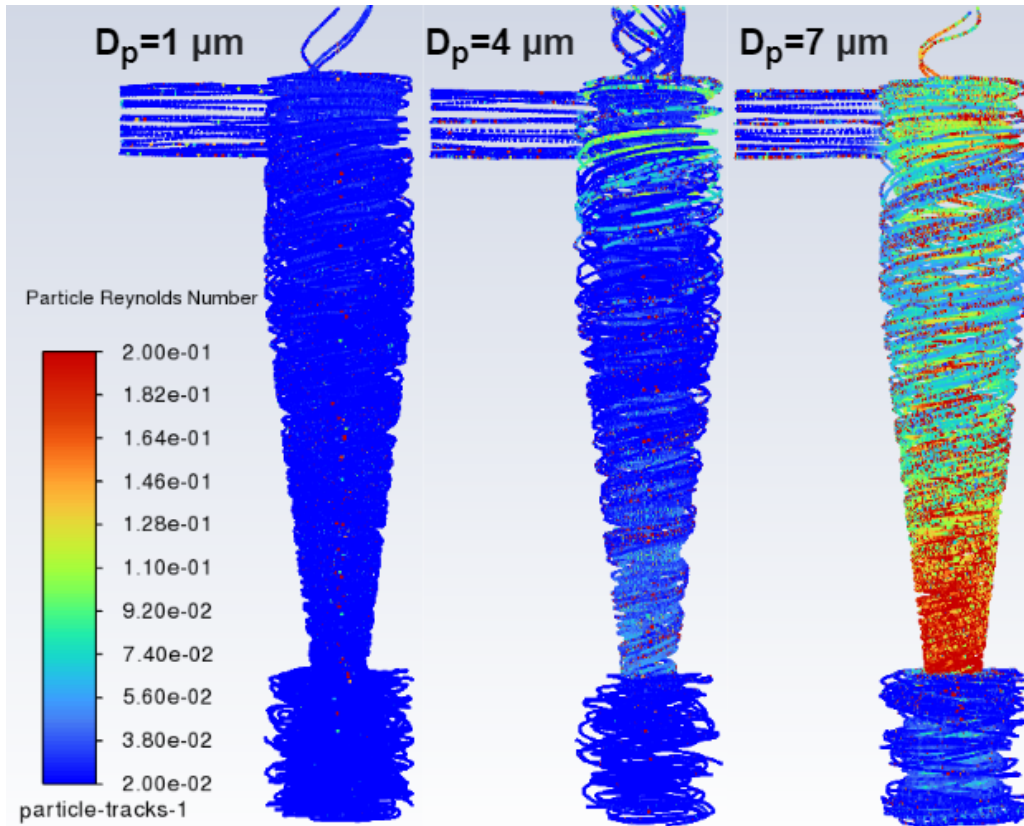
Figure 6.18: Particle Reynolds number for an uniform particle size input of 1, 4 and 7 μm, simulated on D=290 and inlet velocity of 16.34 m/s. Scale from 0.02 to 0.2 Re_p.

Majumder, Yerriswamy, and Barnwal [20] attributed the fishhook effect to a sudden drop in settling velocity, caused by the shift between the transitional to the Stokes regime, which occurs at approximately Re_p<0.2.

It can be seen in Figure 6.18 that the particle Reynolds number at the bottom of the cyclone is approximately in this range, with particle Reynolds number exceeding 0.2 at the bottom of the cyclone for particles sizes between 4 and 7 μm.

This was also tested for a larger cyclone, with a lower inlet velocity, and it showed the same general tendency with the beginning point of the fishhook having a Reynolds number of approximately 0.2.

This supports the hypothesis that the settling velocity of the particles could be the reason for the fishhook effect. The fishhook beginning at a constant Stokes number and an also approximate constant Reynolds particles number is likely due to the close relation between the two, both describing the particle flow conditions. This knowledge of the fishhook occurring at a constant Stokes number can be used to scale the cyclones to fit into a multi cyclone system to get a high overall efficiency.

6.7   Multi Cyclone

The separation efficiency of several cyclones in series will improve the overall separation efficiency for a system. In this section, such methods will be utilised, as well as the fishhook that occurs in the cyclone separators, in order to investigate how it affect the total separation efficiency and pressure loss.

The knowledge of the Stokes scaling can be used to design a system of multi cyclones that has a high overall efficiency. This is done by combining two cyclones, a small and a larger one.

It is then wanted that the two separation efficiency curves overlap so that the point of rise in efficiency due to fishhook on the large cyclone intersect with the decrease in separation efficiency of the small cyclone. This would give the multi cyclone system a high overall efficiency.

An example of a possible combination of multi cyclones can be seen in Figure 6.19.
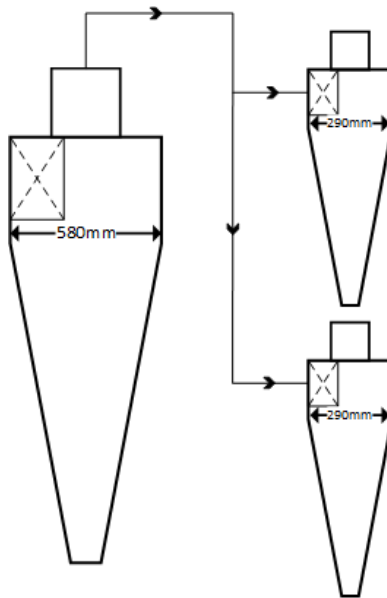6.19.

Figure 6.19: Example of multi cyclone system

Here two of the cyclones from Section 6.6 are used. The Stairmand cyclone with a larger diameter ($D = 580mm$) is simulated with an inlet velocity of $8.17m/s$. From this the escaped particles and pressure loss is noted. In order to match the volumetric flow two cyclones with a diameter of 290 mm and an inlet velocity of 16 m/s are needed.

The overall efficiency of the multi cyclones are found by multiplying the output of the larger Stairmand cyclone ($D = 580mm$) with the separation efficiency of the smaller Stairmand cyclone ($D = 290mm$), in order to calculate the final particle output. The results of this can be seen in figure 6.20.
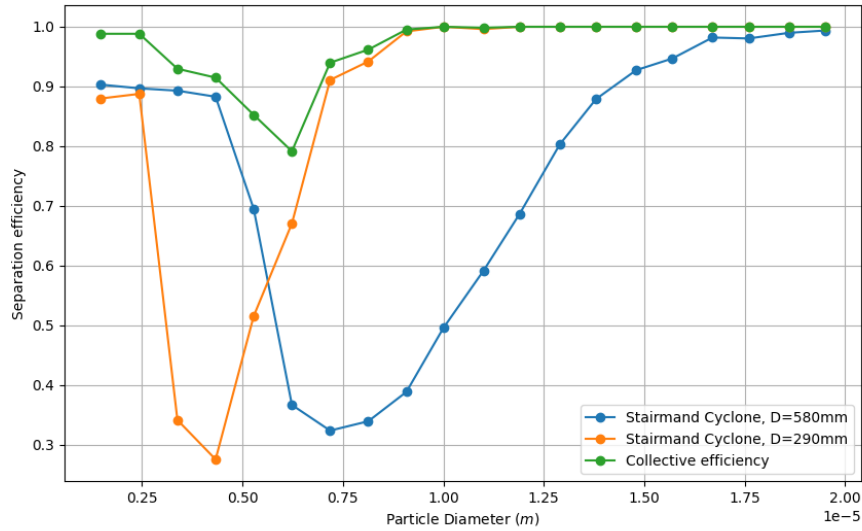
Figure 6.20: Separation efficiency of the separate cyclone together with a combined system separation efficiency.

It can be seen that the fishhook of the larger cyclones overlaps, where the smaller cyclone has a lower efficiency. Meanwhile the small cyclone collects all the larger particles that the larger cyclone does not collect. This results in an overall efficiency of 94.3% for the combined system. The total pressure loss for the system is found to 1073 Pa.

It can be seen that there is a decrease in efficiency on the overall efficiency between 2.5 and 7.5μm, where they do not overlap well. The Stokes scaling law can be utilised to find a point where the overlap is increased, in order to increase the overall efficiency.

6.7.1 Multi Cyclone System Design Using Stokes Scaling

The stokes scaling assumes that the separation efficiency is similar for equal Stokes numbers, for geometrically similar cyclones

In this case the cyclone of $D = 580$ mm is again used. This time the knowledge of the separation efficiency of one cyclone is used to calculate where the efficiency curves should overlap. It was chosen that the efficiency curves should intersect where both have an efficiency of approximately 70%. This would give the system a separation efficiency of above 90% at all diameters. An illustration of this is can be seen in Figure 6.21, with the wanted intersection points, one and two.
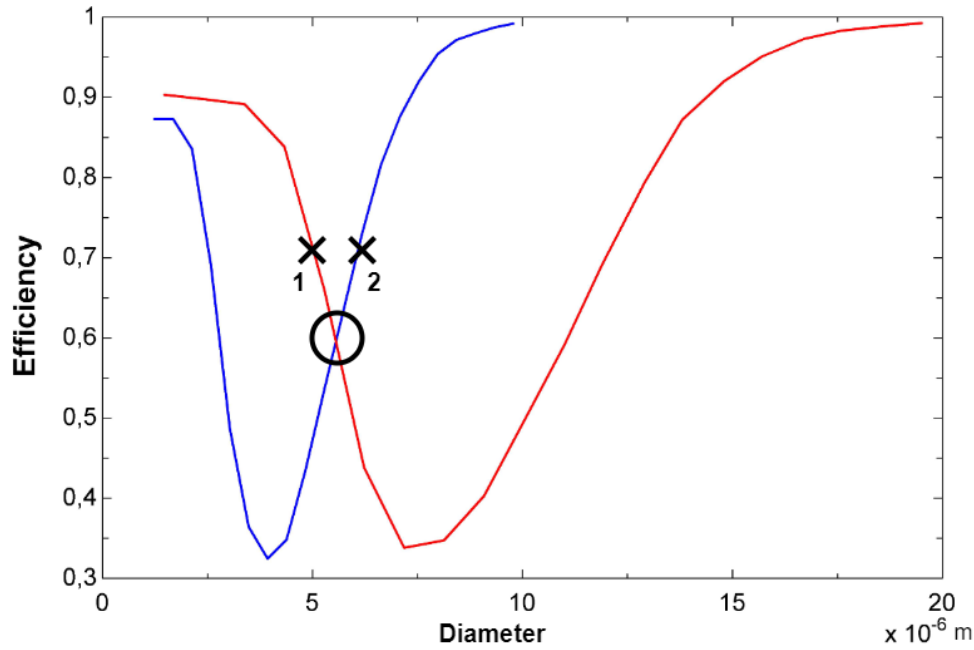
Figure 6.21: Illustration of where the efficiency curves will be calculated to intersect.

To limit the pressure loss the large cyclone of $D = 580$ will be simulated with a velocity of 4.1 m/s, which is half of the previous example. This will shift the efficiency curve to the right and therefore the calculated intersection will also shift to the right. By shifting the intersection to higher particle diameters the velocity in the smaller cyclone can be lowered and therefore limit the pressure loss.

The intersection is calculated by using Stokes scaling from the Stairmand $D = 290$ mm, to find the stokes number at the two points that is wanted to intersect and then setting the particle diameters equal.

$$Stk_{1;D=290} = \frac{v_{580} \cdot x_1^2}{D_{580}} \qquad\qquad Stk_{2;290} = \frac{v_{small} \cdot x_2^2}{D_{small}}$$

$$x_1 = x_2 \tag{6.2}$$

The specific diameter and velocity of the small cyclones are related through the volumetric flow of the larger cyclone. Therefore, their size and flow rate are determined by the number of cyclones the air stream is split up into.

With more cyclones, lower velocity is needed to reach the specific Stokes number and therefore has a lower pressure loss. When designing a multi cyclone system it would ultimately be a compromise or optimization task between efficiency, pressure loss and the number of cyclones.

For this system the stream will be split into two cyclones. This results in a diameter of 262 mm with an inlet

velocity of 10.2 m/s. The two curves should then cross at a diameter of 7.3 μm. The simulated results can be seen in Figure 6.22.
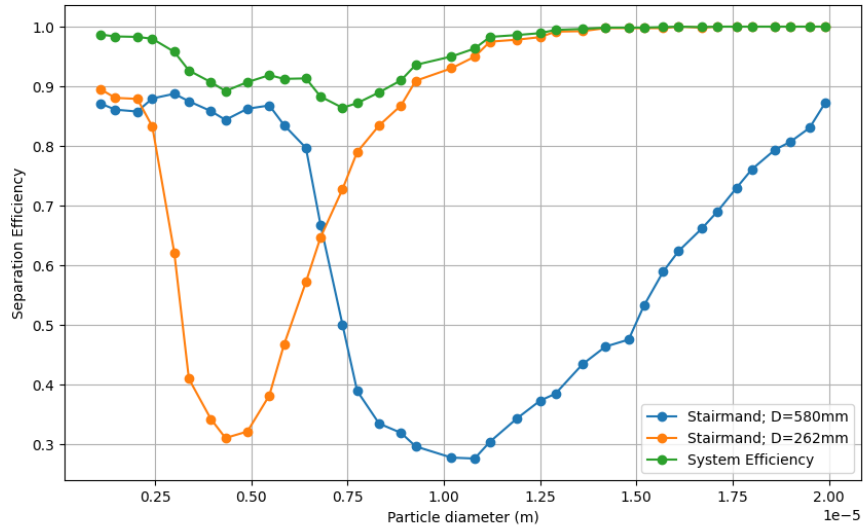

Figure 6.22: Separation efficiency of the separate cyclone together with a combined system separation efficiency.

It can be seen that the curves overlap at 6.8 μm with a minimum separation efficiency of 86.5 %. The overall efficiency of the the system is 91.8 %. The small cyclone had a pressure loss of 333 Pa, while the large cyclone had a pressure loss of 54 Pa. This gives a combined system pressure loss of 387 Pa. It can be seen that the large cyclone in general has a low separation efficiency across a larger range of particle diameters. However the large cyclone fulfills its purpose of separating out a large fraction of the small particles and doing so with a low pressure loss.

If this is compared to the previous multi cyclone system example, this system could replace that system but would require more cyclones to maintain the same volumetric flow. To maintain the same flow two large cyclones and four small ones would have to replace that system. This would maintain a similar overall efficiency, but reduce the pressure loss by 64%

This shows that the overlap of the fishhook is possible to optimize for a required minimum separation efficiency, but a optimization of pressure loss, efficiency and number of cyclones would need to be found.

7 Discussion

System Implementation

There are several factors that can affect the efficiency and performance in a system. As shown in section 6.3, the inlet velocity heavily affects the separation efficiency and pressure loss. In this project the system is designed for a specific workload, and if it is incorporated in a ventilation system with a varying workload it might have a negative impact on the performance. A change in volumetric flow could be countered by possibly implementing a bypass system and simply utilizing the number of cyclones best fitted to the work load in question, while still maintaining the desired separation efficiency and pressure loss. With varying flow, the system should be designed with some safety margin for the efficiency overlap to insure a high separation efficiency for all desired diameters.

Furthermore, for this project it is assumed that the particles does not affect the primary phase due to the low solids loading. For a system with a larger solid loading the particles would impact the flow in the cyclone and also change the fishhook effect as shown in section 5.7.1 by Hoffmann and Stein [15]. This is would change optimum of the efficiency overlapping. This system idea is therefore best suited for a system which operate at constant volumetric flow and low solid loading. To insure a low solid loading, a settling chamber or a large cyclone could be placed upstream of the multi cyclone system to filter out the majority of the particles. The possibility of replacing a bag filter with a series of cyclones will depend on the purpose and requirements of the system. A series of cyclones can separate a high percentage of particles out, but it is harder to guarantee a certain separation efficiency.

Mesh Considerations

Since several simulations focus on the backflow, as well as the vortex finder in general, and how this affect the particle separation, it could be advantageous to refine the mesh in the vortex finder. This could possibly yield more accurate depictions of the behaviour of backflow, and particles in the vortex finder. This was, however, not done for this project due to the limited time frame for the project.

Fishhook Effect

Due to the lack of experimental results from the particle separation of the Stairmand cyclone, it could prove beneficial to test the particle separation of the setup, and compare to the CFD simulations. This would be done in order to validate the particle separation simulated using CFD. It is still uncertain why the fishhook effect is occurring, but based on the simulations in this project, it can be concluded that it is not due to agglomeration or other particle-particle interactions, but rather is occurring at a certain particle Stokes number.

The reason for this rise in separation efficiency, at this specific Stokes number, is still uncertain. It is however, expected to be related to a change from the transitional to the Stokes regime, as explained by Majumder,

Yerriswamy, and Barnwal [20]. This regime change is based on the particle Reynolds number of around 0.2. It was investigated lightly, and a connection between the shift in regime, and beginning of the fishhook effect was found. This would need further and a more thorough investigation to be certain whether this is a reoccurring phenomenon or is only the case for the specific simulation that was investigated.

8 Conclusion

In this project a High Efficiency Stairmand cyclone, was modeled and tested in several ways, order to investigate the possibility of a multi cyclone system replacing a cloth filter system. It was found that the fishhook effect on the particle separation efficiency could play a major role in this task.

An investigation was made to determine the origin of the fishhook effects and how it could be affected. Some of the theories of what causes the fishhook, attribute this to particle-particle interaction, but since this is not modeled in the CFD, it is assumed to be due to the flow conditions. It was therefore investigated what could influence this.

It was found that a cyclone separator with a smaller vortex finder diameter, lead to an increase in both pressure loss and separation efficiency, due to a limited number of particles that short circuit in the system. It did, however, not significantly change the fishhook effect. It was also tried to include a bend on the outlet of the cyclone to investigate how this impacted the backflow and pressure loss. This did not hinder backflow or change the separation efficiency significantly, but increased the pressure loss. Various inlet velocities were also tested in order to investigate how this affects the backflow, pressure loss and separation efficiency of the cyclone. It was found that the backflow was proportional to inlet velocity and that the inlet velocity could shift the fishhook effect to different particle sizes.

Furthermore the cyclone was geometrically scaled with varying inlet velocities. From this it was found that the fishhook effect occurred at a constant Stokes number. Meaning that the fishhook in the efficiency curve can be scaled and optimized according to the Stokes scaling laws.

From this, it was hypothesised that a series of cyclones, with various sizes and inlet velocities, can improve the separation efficiency as well as the pressure loss of a system. This was achieved by utilizing the overlap in the efficiency curves due to the fishhook effect occurring at different particle sizes in different cyclones.

An optimization task, determining the optimum pressure loss and number of cyclones from a required separation efficiency would have to be made for a given system. A possible system design was made, consisting of a large and two smaller cyclones, with minimum separation efficiency of 86.5% across particle diameters 1-20 μm, with limited pressure loss. The system is, however, dependent on constant operating parameters, to maintain desired performance.

It should be noted that this is purely based on theoretical calculations and simulations, which applies certain assumptions that may cause a deviation from a practical application. Therefore it would prove valuable to make a physical experiment to test the credibility of these results.

Bibliography

[1] ANSYS. *Ansys Fluent Theory Guide*. `https://dl.cfdexperts.net/cfd_resources/Ansys_Documentation/Fluent/Ansys_Fluent_Theory_Guide.pdf`. 2021.

[2] F. Boysan, W.H. Ayers, and Swithenbank. "A fundemental mathematical modelling approach to cyclone design". In: (1982). ISSN: 0046-9858.

[3] Gang Cao et al. "Study on the effect of a new type of deswirler on the flow field and performance of a cyclone separator". In: (2024).

[4] Ismail B. Celik et al. "Procedure for Estimation and Reporting of Uncertainty Due to Discretization in CFD Applications". In: *Journal of Fluids Engineering* 130 (2008). DOI: `10.1115/1.2960953`. URL: `https://asmedigitalcollection.asme.org/fluidsengineering/article/130/7/078001/444689/Procedure-for-Estimation-and-Reporting-of`.

[5] Zhuo Lun Cen, Ji Gang Zhao, and Ben Xian Shen. "A Comparative Study of Omega RSM and RNG k–epsilon Model for the Numerical Simulation of a Hydrocyclone". In: *IRANIAN JOURNAL OF CHEMISTRY & CHEMICAL ENGINEERING-INTERNATIONAL ENGLISH* 33 (2014). DOI: `1021-9986/14/3/`.

[6] J. M. Cimbala. "Drag on Spheres". In: (2012). URL: `https://www.me.psu.edu/cimbala/me325web_Spring_2012/Labs/Drag/intro.pdf`.

[7] JKF Industries Development Department. *Personal Communication*. 17/04/2024.

[8] DCE – Nationalt Center for Miljø og Energi. *LUFTKVALITET 2020-Status for den nationale luftkvalitetsovervågning i Danmark*. 2020.

[9] Richard C. Flagan and John H. Seinfeld. *Fundamentals of air pollution engineering*. Prentice-Hall, Inc, 1988. ISBN: 0-486-48872-1.

[10] P.A. Funk. "Reducing cyclone pressure drop with evasés". In: *Powder Technology* 272 (2015), pp. 276–281. DOI: `10.1016/j.powtec.2014.12.019`.

[11] A. Haider and O.Levenspiel. "Drag coefficient and terminal velocity of spherical and nonspherical particles". In: *Powder Technology* 58 (1988), pp. 63–70. DOI: `10.1016/0032-5910(89)80008-7`.

[12] Yassin A. Hassan. *Thermal-Hydraulics of Water Cooled Nuclear Reactors*. 1st. Woodhead Publishing, 2017. ISBN: 978-0-08-100662-7.

[13] Niels Henrik Hassing. *Prediction of Flow in Gas Cyclones*. Institute of Energy Technology AAlborg University, 1993. ISBN: 8789179099.

[14] Arjen Hoekstra. *Gas Flow Field and Collection Efficiency of Cyclone Seperators*. Springer, 2000. ISBN: 90-90143341-3.

[15] A.C. Hoffmann and L.E. Stein. *Gas Cyclones and Swirl Tubes*. second edition. Springer, 2008. ISBN: 978-3-540-74694-2.

[16] E.I. Idel'chik. *Handbook of Hydraulic Resistance*. Israel Program for Scientific Translations, 1966.

[17] Donna Lee Iozia and David Leith. "Effect of cyclone dimensions on gas flow pattern and collection efficiency". In: *Aerosol Science and Technology* 10 (1989), pp. 491–500. DOI: `10.1016/0304-3967(80)90007-4`.

[18] Thomas Nørregaard Jensen, Peter Rebsdorf, and Peter Bøgh Pedersen. *Udvikling af multicyklon til reduktion af luftforurening med fine støvpartikler*. Teknologisk Institut, 2017.

[19] Dana Loomis, Wei Huang, and Guosheng Chen. "The International Agency for Research on Cancer (IARC) evaluation of the carcinogenicity of outdoor air pollution: focus on China". In: *Chinese Journal of Cancer* 33 (2014), pp. 189–196. DOI: `10.5732/cjc.014.10028`. URL: `https://www.ncbi.nlm.nih.gov/pmc/articles/PMC3975184/`.

[20] A.K. Majumder, P. Yerriswamy, and J.P. Barnwal. "The "fish-hook" phenomenon in centrifugal separation of fine particles". In: *Minerals Egineering* 16 (2003), pp. 1005–1007. DOI: `10.1016/j.mineng.2003.07.001`.

[21] Efstathios Michaelides, Clayton T. Crowe, and John D. Schwarzkopf. *Multiphase Flow Handbook*. CRC Press, 2016. ISBN: 9781498701006.

[22] Dzmitry Misiulia, Khairy Elsayed, and Anders Gustav Andersson. "Geometry optimization of a deswirler for cyclone separator in terms of pressure drop using CFD and artificial neural network". In: *Separation and Purification Technology* 185 (2017), pp. 10–23. DOI: `10.1016/j.seppur.2017.05.025`.

[23] Dzmitry Misiulia et al. "High-efficiency industrial cyclone separator: A CFD study". In: *Energy* 364 (2019), pp. 943–953. DOI: `10.1016/j.powtec.2019.10.064`. URL: `https://www.sciencedirect.com/science/article/pii/S0032591019308873`.

[24] A.J. Morsi and S.A. Alexander. "An Investigation of Particle Trajectories in Two-Phase Flow System". In: *Journal of Fluid Mechanics* 55 (1972), pp. 193–208. DOI: `10.4209/aaqr.2013.04.0129`.

[25] Canadian Centre of Occupational Health and Safety. "How Do Particulates Enter the Respiratory System". In: (2023). URL: `https://www.ccohs.ca/oshanswers/chemicals/how_do.html`.

[26] Thomas J. Overcamp and Steven E. Scarlett. "Effect of Reynolds Number on the Stokes Number of Cyclones". In: *Aerosol Science and Technology* 19 (1993), pp. 362–370. DOI: `10.1080/02786829308959643`.

[27] E.J. Roldán-Villasana, R.A. Williams, and T. Dyakowski. "The origin of the fish-hook effect in hydrocyclone separators". In: *Powder Technology* 77 (1993), pp. 243–250. DOI: `10.1016/0032-5910(93)85017-4`.

[28] Francisco José de Souza, Ricardo de Vasconcelos Salvo, and Diego de Moro Martins. "Effects of the gas outlet duct length and shape on the performance of cyclone separators". In: *Separation and Purification Technology* 142 (2015), pp. 90–100. DOI: `10.4209/aaqr.2013.04.0129`.

[29] D.B. Spalding. "A single formula for the law of the wall". In: *Journal of Applied Mechanics* 28 (1961), pp. 455–458. DOI: `10.1115/1.3641728`.

[30] Xun Sun et al. "Multi-objective optimization of a Stairmand cyclone separator using response surface methodology and computational fluid dynamics". In: *Powder Technology* 320 (2017), pp. 51–65. DOI: 10.1016/j.powtec.2017.06.065. URL: https://www.sciencedirect.com/science/article/pii/S0032591017305338.

[31] Xun Sun et al. "Multi-objective optimization of a Stairmand cyclone separator using response surface methodology and computational fluid dynamics". In: *Powder Technology* 320 (2017), pp. 51–65. DOI: 10.1016/j.powtec.2017.06.065. URL: https://www.sciencedirect.com/science/article/pii/S0032591017305338.

[32] L. Svarovsky. *Hydrocyclones*. Holt, Rinehart and Winston East Sussex, 1984.

[33] Fuat Tan, Irfan Karagoz, and Atakan Avci. "Effects of Geometrical Parameters on the Pressure Drop for a Modified Cyclone Separator". In: *Chemical Engineering & Technology* 39 (2015), pp. 576–581. DOI: 10.1002/ceat.201500182.

[34] S. Venkatesh et al. "Performance investigation of the combined series and parallel arrangement cyclone separator using experimental and CFD approach". In: *Powder Technology* 361 (2020), pp. 1070–1080. DOI: 10.1016/j.powtec.2019.10.087. URL: https://www.sciencedirect.com/science/article/pii/S0032591019309167?via%3Dihub.

[35] H.K. Versteeg and W. Malalasekera. *An introduction to computational fluid dynamics - The finite volume method*. Pearson Education, 2007.

[36] P.Aarne Vesilind. "The Rosin-Rammler particle size distribution". In: *Resource Recovery and Conservation* 5 (1980), pp. 275–277. DOI: 10.1016/0304-3967(80)90007-4.

[37] Adam Voiland. "How Dust Affects the World's Health". In: (2023). URL: https://earthobservatory.nasa.gov/images/151100/how-dust-affects-the-worlds-health.

[38] Xiaoyan Wang et al. "Study on horizontal turbine classification". In: *Powder Technology* 102 (1999), pp. 166–170. DOI: 10.1016/S0032-5910(98)00206-X.

[39] Aidan Wimshurst. "What is the difference between y+ and y*". In: (2019). URL: https://www.youtube.com/channel/UCcqQi9LT0ETkRoUu8eYaEkg.

[40] Weiwei Xu et al. "Performance evaluation of a new cyclone separator – Part II simulation results". In: *Separation and Purification Technology* 160 (2016), pp. 112–116. DOI: 10.1016/j.seppur.2016.01.012. URL: https://www.sciencedirect.com/science/article/pii/S1383586616300120?via%3Dihub.

[41] Pan Zhang et al. "Analysis of the nutation and precession of the vortex core and the influence of operating parameters in a cyclone separator". In: *Chinese Journal of Chemical Engineering* 46 (2022), pp. 1–10. ISSN: 1004-9541. DOI: https://doi.org/10.1016/j.cjche.2021.05.016. URL: https://www.sciencedirect.com/science/article/pii/S1004954121002536.